A novel search strategy for right-handed charged gauge bosons at the Large Hadron Collider

Mariana Frank ⓘ,[a] **Benjamin Fuks** ⓘ,[b] **Adil Jueid** ⓘ,[c] **Stefano Moretti** ⓘ[d,e] **and Özer Özdal** ⓘ[a,d]

[a]*Department of Physics, Concordia University,*
7141 Sherbrooke St. West, Montreal, Quebec H4B 1R6, Canada

[b]*Laboratoire de Physique Théorique et Hautes Énergies (LPTHE), UMR 7589,*
Sorbonne Université & CNRS, 4 place Jussieu, 75252 Paris Cedex 05, France

[c]*Particle Theory and Cosmology Group, Center for Theoretical Physics of the Universe,*
Institute for Basic Science (IBS),
Daejeon, 34126, Republic of Korea

[d]*School of Physics & Astronomy, University of Southampton,*
Highfield, Southampton SO17 1BJ, U.K.

[e]*Department of Physics & Astronomy, Uppsala University,*
Box 516, 75120 Uppsala, Sweden

E-mail: mariana.frank@concordia.ca, fuks@lpthe.jussieu.fr,
adiljueid@ibs.re.kr, stefano.moretti@cern.ch, ozer.ozdal@soton.ac.uk

ABSTRACT: We explore the potential of the Large Hadron Collider (LHC) in detecting a signal originating from the production of a heavy $SU(2)_R$ charged gauge boson that then decays into a top-bottom quark pair via the mediation of a right-handed neutrino, $pp \to W_R \to N_R \ell \to (\ell' tb)\ell$. Such a channel, that we study in the context of the minimal Left-Right Symmetric Model, contrasts with conventional smoking-gun signatures targeted experimentally and phenomenologically in which only light quarks are involved. We propose a selection strategy aimed at extracting such a top-bottom signal and we estimate the resulting sensitivity of the LHC to the model. Our results demonstrate the potential impact of such a search and we therefore urge the experimental collaborations to carry out a similar analysis in the light of present and future data.

Contents

1 Introduction

The Standard Model (SM) of particle physics is unable to address fundamental questions in Nature despite being in excellent agreement with all measurements carried out at experiments so far. For instance, the origin of parity violation in electroweak (EW) interactions remains a mystery to which the SM has no answer. Left-Right Symmetric Models (LRSMs) are one of the most attractive solutions to such a problem [1–4]. Their minimal incarnation is dubbed the minimal LRSM (mLRSM). It is based on the $\mathrm{SU}(2)_L \otimes \mathrm{SU}(2)_R \otimes \mathrm{U}(1)_{B-L}$ gauge group, and it predicts a particle spectrum comprising several extra states, including new charged and neutral gauge bosons, extra (pseudo)scalars (i.e. neutral, singly-charged and doubly-charged bosons), and three generations of right-handed neutrinos. Furthermore, this minimal model accommodates naturally small neutrino masses through the seesaw mechanism [5–7], it elegantly addresses the problem of parity violation, and it has a rich phenomenology both at colliders and relative to low-energy experiments. The presence of extra right-handed charged-currents and new (pseudo)scalar interactions indeed impact lepton flavour violation in charged lepton decays and $e \to \mu$ conversions [8], EW precision observables [9–11], Charge-Parity (CP) violations in meson decays and meson-antimeson oscillations [12–19], electric dipole moments of various particle types [20–24], and nuclear β decays [25, 26]. In particular, a recent comprehensive global analysis of the mLRSM by means of low-energy observables has been carried in ref. [27], while the consequences on its leptonic and (pseudo)scalar sectors have been analysed in refs. [28–34] and [35–38] respectively. In

contrast to other models featuring multi-Higgs doublets, the extra (pseudo)scalar states of the mLRSM originate from an $SU(2)_L \otimes SU(2)_R$ bi-doublet, and it has been shown that they need to be as heavy as $\mathcal{O}(10)\,\text{TeV}$ to avoid large flavour-changing neutral-current transitions.

The mLRSM also predicts lepton number violation that contribute to neutrinoless double-beta ($0\nu\beta\beta$) decay rates. Such contributions are highly correlated with the neutrino mass parameters and the $SU(2)_R$ gauge boson masses, while being amenable to discovery even for small neutrino masses (see refs. [39–42] for recent analyses). The mLRSM correspondingly features high-energy analogues of the usual low-energy $0\nu\beta\beta$ processes. One of them consists of the so-called Keung-Senjanovic mechanism that is expected to occur at high-energy hadron colliders [43]. The idea is that on-shell and off-shell $SU(2)_R$ gauge bosons, denoted in what follows as W_R, can decay into a lepton and right-handed neutrino N_R that itself further decays into two light quarks and another (charged) lepton. If the two charged leptons have the same electric charge, then this process breaks lepton number conservation by two units, providing therefore a direct correlation with the rates of $0\nu\beta\beta$ decays. Furthermore, the production of opposite-sign charged leptons is also interesting on its own [44–47], which has consequently motivated the ATLAS and CMS collaborations to carry out several searches for a W_R state at the Large Hadron Collider (LHC), both in the same-sign and opposite-sign dileptonic channels [48–52]. Depending on the N_R mass and the lepton flavour structure, W_R-boson masses up to 4.8–$5.0\,\text{TeV}$ are excluded today [52].[1] Furthermore, at large momentum transfer the same $0\nu\beta\beta$ matrix elements imply several enhancements in the production rates of same-sign lepton pairs of possibly different flavours via vector-boson scattering [55–58]. Constraints on heavy neutrinos with masses in the $50\,\text{GeV}$ — $20\,\text{TeV}$ range can here be imposed, hence even above the LHC energy scale.

In the light of these efforts, an interesting question, that was also raised in ref. [59], arises: *what if we use heavy quarks instead of light ones in searching for W_R and N_R states?* In this case the produced N_R particle undergoes a three-body decay into a charged lepton, a bottom quark, and a top quark, leading thus to a very rich final state. This consists of an intriguing signature, as it is widely believed that the top quark can play an important role in probing new physics Beyond the SM (BSM).

The aim of this study is to propose a *novel* search strategy for the production of an $SU(2)_R$ charged gauge boson W_R and a neutrino N_R at the LHC, relying on the $W_R \to N_R\ell \to tb\ell\ell$ decay chain with the W_R emerging from charged current Drell-Yan (DY) production. The top quark, being produced from a heavy neutrino decay, is highly boosted in most of the cases. Jet substructure methods and top taggers have therefore the potential to efficiently reduce the SM background, together with specific kinematics variables exploiting the richness of the final state. The use of this channel can thus be crucial not only for discovery purposes but also for diagnostics as a probe of the properties of the mLRSM as a whole.

The rest of this paper is organised as follows. In section 2 we briefly discuss the mLRSM, its field content and the associated Lagrangian, and we assess the constraints emerging from recent searches for W_R bosons and N_R neutrinos at colliders (with some technical details on the reinterpretation of the LHC results being reported in appendix A). Next we

---

[1]These bounds can be relaxed in cases where the W_R boson couples in a generic way to leptons and quarks, i.e. when $g_L \neq g_R$ (see e.g. refs. [53, 54]).

study W_R and N_R production and decay in the $\ell\ell tb$ channel in section 3, where we also present our signal and background analysis, and its results. The latter include an estimation of the sensitivity of the LHC to the mLRSM signal considered, and we demonstrate the potential usefulness of designing corresponding searches in real LHC data. We conclude and summarise our work in section 4.

2 The model and current bounds

2.1 The model

In this section, we briefly describe the mLRSM, its particle content, and the interaction Lagrangian relevant for our analysis (more technical details can be found in refs. [60–64]). The fermion sector of the mLRSM includes the following fields:

$$q_L \equiv \begin{pmatrix} u_L \\ d_L \end{pmatrix}_{(\mathbf{2},\mathbf{1},\frac{1}{3})}, \qquad q_R \equiv \begin{pmatrix} u_R \\ d_R \end{pmatrix}_{(\mathbf{1},\mathbf{2},\frac{1}{3})}, \qquad \ell_L \equiv \begin{pmatrix} \nu_L \\ e_L \end{pmatrix}_{(\mathbf{2},\mathbf{1},-1)}, \qquad \ell_R \equiv \begin{pmatrix} N_R \\ e_R \end{pmatrix}_{(\mathbf{1},\mathbf{2},-1)},$$

(2.1)

in which the subscripts refer to the representation of the fermion fields under $\mathrm{SU}(2)_L \otimes \mathrm{SU}(2)_R \otimes \mathrm{U}(1)_{B-L}$. In addition, we denote the three gauge couplings associated with this gauge symmetry by g_L, g_R, and g_{B-L}. Parity conservation at high scales dictates that the gauge interactions be invariant under

$$\{W_L, q_L, \ell_L\} \longleftrightarrow \{W_R, q_R, \ell_R\}.$$

(2.2)

An immediate consequence of this symmetry is that g_L and g_R are equal, i.e. $g_L \equiv g_R \equiv g$. Thus EW symmetry breaking is minimally achieved through the vacuum expectation values acquired by the neutral components of three scalar multiplets: a bi-doublet (Φ) and two triplets ($\Delta_{L,R}$) represented as:

$$\Phi \equiv \begin{pmatrix} \phi_1^0 & \phi_2^+ \\ \phi_1^- & \phi_2^0 \end{pmatrix}_{(\mathbf{2},\mathbf{2},0)}, \qquad \Delta_L \equiv \begin{pmatrix} \frac{\delta_L^+}{\sqrt{2}} & \delta_L^{++} \\ \delta_L^0 & -\frac{\delta_L^+}{\sqrt{2}} \end{pmatrix}_{(\mathbf{3},\mathbf{1},2)}, \qquad \Delta_R \equiv \begin{pmatrix} \frac{\delta_R^+}{\sqrt{2}} & \delta_R^{++} \\ \delta_R^0 & -\frac{\delta_R^+}{\sqrt{2}} \end{pmatrix}_{(\mathbf{1},\mathbf{3},2)}.$$

(2.3)

The model's Lagrangian $\mathcal{L}$ is given by

$$\begin{aligned} \mathcal{L} = {} & \mathcal{L}_{\text{gauge}} + i\bar{q}_L \slashed{D} q_L + i\bar{q}_R \slashed{D} q_R + i\bar{\ell}_L \slashed{D} \ell_L + i\bar{\ell}_R \slashed{D} \ell_R \\ & + \mathrm{Tr}\Big[(D_\mu \Phi)^\dagger (D^\mu \Phi)\Big] + \mathrm{Tr}\Big[(D_\mu \Delta_L)^\dagger (D^\mu \Delta_L)\Big] + \mathrm{Tr}\Big[(D_\mu \Delta_R)^\dagger (D^\mu \Delta_R)\Big] \\ & - \Big[\bar{q}_L (Y_q \Phi + \tilde{Y}_q \tilde{\Phi}) q_R + \bar{\ell}_L (Y_\ell \Phi + \tilde{Y}_\ell \tilde{\Phi}) \ell_R + \bar{\ell}_L^c i\sigma_2 \Delta_L Y_L \ell_L + \bar{\ell}_R^c i\sigma_2 \Delta_R Y_R \ell_R + \text{H.c.}\Big] \\ & - V(\Phi, \Delta_L, \Delta_R), \end{aligned}$$

(2.4)

where $\mathcal{L}_{\text{gauge}}$ includes kinetic terms for all gauge bosons, $V(\Phi, \Delta_L, \Delta_R)$ is the scalar potential (which exact form is irrelevant for our study), and all Yukawa couplings Y are 3×3 matrices in the flavour space. Moreover, $\tilde{\Phi}$ is the dual bi-doublet Higgs field, and D_μ stands for the covariant derivative operator

$$D_\mu = \partial_\mu - ig T_L^I W_{L,\mu}^I - ig T_R^I W_{R,\mu}^I - i\frac{g_{B-L}}{2} Q_{B-L} B_\mu,$$

(2.5)

– 3 –

with T_L^I and T_R^I being the generators of $\mathrm{SU}(2)_L$ and $\mathrm{SU}(2)_R$ taken in the relevant representation, and Q_{B-L} is the associated $\mathrm{U}(1)_{B-L}$ charge. EW symmetry breaking proceeds in two steps. First, the vacuum expectation value acquired by the triplet Δ_R breaks the $\mathrm{SU}(2)_R \otimes \mathrm{U}(1)_{B-L}$ symmetry down to the hypercharge group $\mathrm{U}(1)_Y$. Second, the bi-doublet Φ and triplet Δ_L Higgs fields choose a configuration breaking the $\mathrm{SU}(2)_L \otimes \mathrm{U}(1)_Y$ symmetry down to electromagnetism. The full corresponding vacuum configuration is hence given by

$$\langle \Phi \rangle = \begin{pmatrix} v_1 & 0 \\ 0 & -v_2 e^{-i\alpha} \end{pmatrix}, \qquad \langle \Delta_{L,R} \rangle \equiv \begin{pmatrix} 0 & 0 \\ v_{L,R} & 0 \end{pmatrix}. \tag{2.6}$$

We further define the mixing angle β such that $v = v_1 \sin\beta = v_2 \cos\beta$, and we enforce the hierarchy $v_L \ll v \ll v_R$ to get agreement with neutrino data (v_L being small) and constraints on additional gauge bosons (v_R being large). In this setup, the masses of the charged gauge bosons read

$$M_{W_L}^2 \approx \frac{1}{2} g^2 v^2, \qquad M_{W_R}^2 \approx g^2 v_R^2. \tag{2.7}$$

## 2.2 Limits on W_R properties from collider and low-energy experiments

Several searches have focused on testing for the existence of W_R bosons associated with the $\mathrm{SU}(2)_L \times \mathrm{SU}(2)_R \times \mathrm{U}(1)_{B-L}$ gauge symmetry. While at tree-level the mixing between the two electrically charged bosons W_L and W_R results in a shift of the W_L mass from its SM value M_W, data indicate that the corresponding mixing angle must be smaller than 10^{-2} [65]. This is consistent with our model configuration in which this mixing is negligible, and in which the W_R boson couples essentially to right-handed fermions. The structure of such a coupling in the flavour space is further dictated by the values of the elements of a Cabibbo-Kobayashi-Maskawa (CKM) matrix relating right-handed fermions, which generally needs not be proportional to the known CKM matrix (that relates left-handed fields).

At hadron colliders searches for signatures of a W_R boson have concentrated on resonant production. The most commonly looked for signal is made up of high-momentum electrons or muons accompanied by a large amount of missing transverse energy, originating from the process

$$pp \to W_R X \to \ell N_R X \qquad \text{with} \qquad \ell = e, \mu, \tau. \tag{2.8}$$

Searches in this channel assume that the narrow width approximation is valid (with the W_R boson width-over-mass ratio $\Gamma_{W_R}/M_{W_R} \leq 7\%$),[2] and that the heavy neutrino N_R is lighter than the W_R boson and escapes detection. Relying on the Sequential Standard Model (SSM) as a benchmark new physics setup, the ATLAS and CMS collaborations have set stringent limits on the W_R boson by making use of $139\,\mathrm{fb}^{-1}$ of data at a centre-of-mass energy $\sqrt{s} = 13\,\mathrm{TeV}$. In the electronic channel, they constrained the W_R boson mass to satisfy $M_{W_R} > 6\,\mathrm{TeV}$, while in the muonic channel the bounds are reduced to $5.6\,\mathrm{TeV}$ [68, 69]. In contrast, limits only reach $M_{W_R} > 5\,\mathrm{TeV}$ for a final state comprising tau leptons. By virtue of the Keung-Senjanovic mechanism, the right-handed neutrino N_R produced through process (2.8) could also decay, through a virtual W_R boson exchange, into an $eejj$, $\mu\mu jj$ or

---

[2]The effects of the W_R-boson width on the signal have been explored in refs. [66, 67].
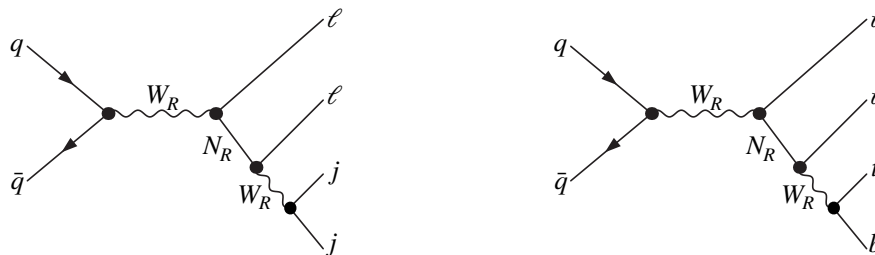
Figure 1. Representative parton-level Feynman diagrams illustrating the production of two leptons and either a pair of jets (left) or a top-bottom system (right) from the decay of a heavy right-handed neutrino N_R. The latter originates from the decay of a possibly off-shell $SU(2)_R$ charged gauge boson W_R emerging from DY production.

$\tau\tau jj$ system. Such a new physics signature was explored by both collaborations, and cross section limits as functions of the N_R and W_R masses have been determined from 13 TeV LHC data [49, 52, 70]. This is further addressed in section 2.4.

Searches for di-jet resonances can also be used to set bounds on the signal originating from the process $pp \to W_R \to q\bar{q}'$. Within the SSM, limits on the W_R boson mass of 4 TeV have been obtained [52, 71]. On the other hand, The ATLAS collaboration also excluded M_{W_R} lighter than 3.25 TeV from $pp \to W_R \to t\bar{b} + \text{h.c.}$ using 36 fb^{-1} of integrated luminosity [72]. Furthermore, both collaborations have searched for the signal that would emerge from the processes $pp \to W_R \to ZW_L$ and $pp \to W_R \to HW_L$ in all possible final states (leptonic, semi-leptonic and hadronic), and derived that $M_{W_R} \geq 3.9$ TeV [73, 74].

On different grounds, mass limits on W_R bosons can also be obtained indirectly from low-energy constraints, especially from box diagrams contributing to kaon mixing. In the case where the CKM matrices in the right-handed and left-handed quark sectors are the same, we get $M_{W_R} > 2.9$ TeV [75]. Parity violation effects to be observed in polarised muon decays additionally impose that $M_{W_R} > 600$ GeV [76], and combined limits on M_{W_R} and M_{N_R} can be additionally derived [28].

2.3 Production of W_R bosons at the LHC

We consider the DY-like production of a (possibly off-shell) W_R boson in *pp* collisions, followed by its decay via the Keung-Senjanovic mechanism into two charged leptons and either two jets or a top-bottom system,

$$pp \to W_R \to \ell N_R \to \ell\ell jj \qquad \text{or} \qquad pp \to W_R \to \ell N_R \to \ell\ell tb. \tag{2.9}$$

In our notation, j represents a light jet resulting from the fragmentation of quarks or antiquarks from the first or second generation, and ℓ stands for either an electron or a muon. Moreover, among all possible flavour and electric-charge assignments for the two leptons, we restrict our analysis to the case of a Same-Sign (SS) and Opposite-Sign (OS) lepton pair of the Same Flavour (SF). Representative parton-level Feynman diagrams illustrating the processes (2.9) are shown in figure 1. In the following, we consider an mLRSM scenario in which the right-handed neutrino is lighter than the W_R gauge boson ($M_{N_R} \leq M_{W_R}$), and we set the two CKM matrices to the 3×3 identity matrix.

We begin with a calculation of the cross section for the first of the processes (2.9), $pp \to \ell N_R \to \ell\ell jj$, both at Leading Order (LO) and Next-to-Leading Order (NLO) in
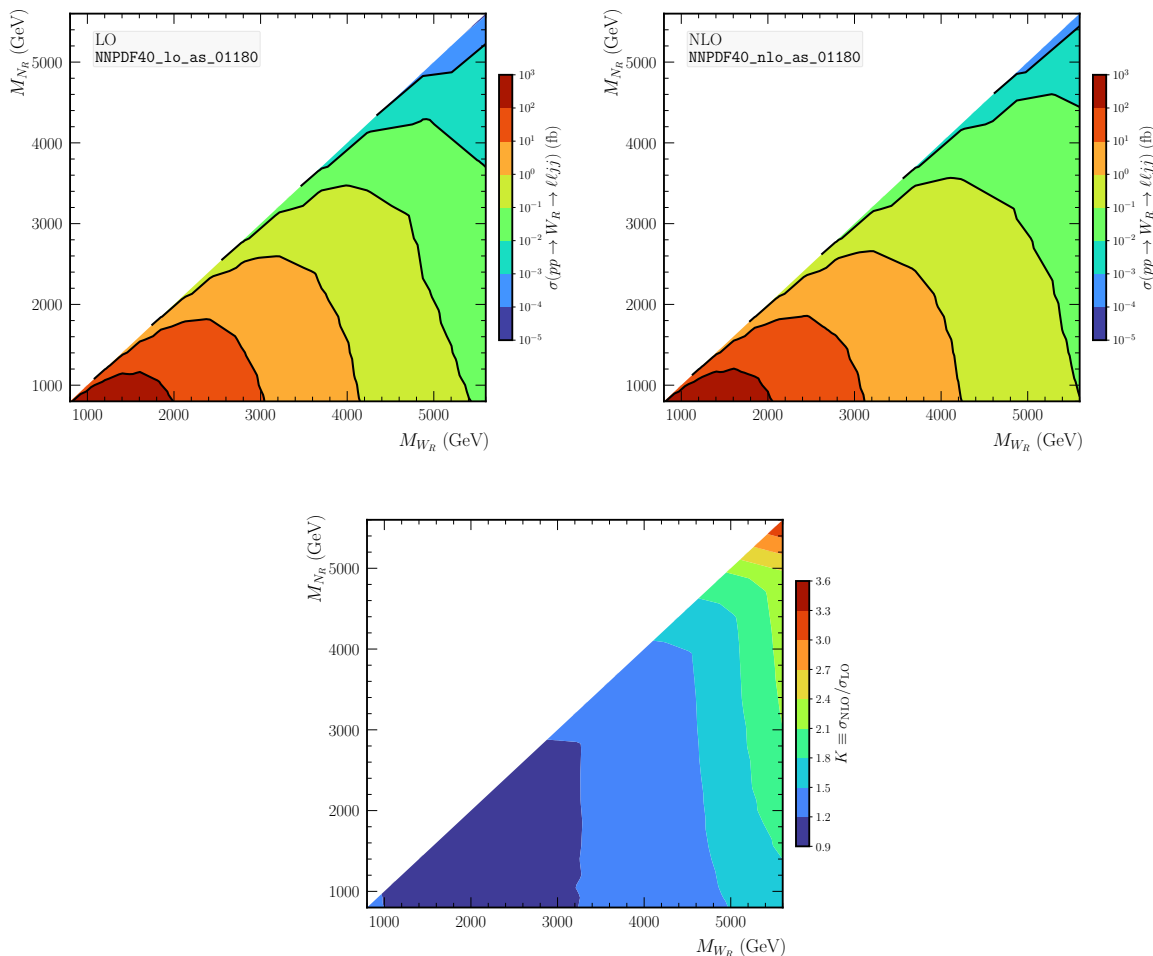
Figure 2. Production cross sections related to the process $pp \to W_R \to \ell N_R \to \ell\ell jj$ at LO (top row, left) and NLO (top row, right), for a centre-of-mass energy $\sqrt{s} = 13$ TeV. We also display the K-factor defined as in (2.10) (bottom row).

QCD. We rely on the narrow-width approximation so that we can factorise the full process into a 'production part' ($pp \to \ell N_R$) and a 'decay part' ($N_R \to \ell jj$). The generation of the corresponding 'production' LO and NLO matrix elements is achieved by means of MADGRAPH5_AMC@NLO version 3.4.2 [77] and a UFO [78, 79] implementation of the relevant sectors of the mLRSM. The latter is obtained by means of FEYNRULES [80, 81] and NLOCT [82], and an in-house effective implementation of the Lagrangian (2.4) that considers only the W_R-boson interactions with fermions and the SM sector (on the same grounds as in the parametrisation proposed in ref. [83]). The 'decay' matrix elements are instead always evaluated at LO thanks to MADSPIN [84], which allows us to keep track of all spin correlations inherent to the fermionic nature of the right-handed neutrino N_R and its decay products. Hadronic cross sections are next obtained by convoluting the resulting 'full' matrix elements with the LO (`NNPDF40_lo_as_01180`) and NLO (`NNPDF40_nlo_as_01180`) sets of NNPDF 4.0 Parton Distribution Functions (PDFs) [85] for LO and NLO calculations, respectively, and this relies on a central scale choice in which both the factorisation and

renormalisation scales are fixed to the W_R-boson mass, $\mu_R = \mu_F = M_{W_R}$. To visualise the size of the NLO corrections, we define a global K-factor by the ratio of the LO to NLO rates $\sigma_{\text{LO}} \equiv \sigma(pp \to \ell\ell jj)_{\text{LO}}$ and $\sigma_{\text{NLO}} \equiv \sigma(pp \to \ell\ell jj)_{\text{NLO}}$,

$$K \equiv \frac{\sigma_{\text{NLO}}}{\sigma_{\text{LO}}}. \tag{2.10}$$

Production cross sections for the 'full' process $pp \to \ell N_R \to \ell\ell jj$ are displayed in figure 2 at LO (top row, left) and NLO (top row, right), together with the associated K-factors as defined in (2.10) (bottom row). They are found to vary between 100–1000 fb for a relatively light W_R boson with a mass between 1 and 2 TeV, to around 10^{-3} fb for a very heavy W_R boson with a mass around 5 TeV, i.e. in the vicinity of the exclusion limits relevant for a sequential extra charged gauge boson (the precise reinterpretation of these bounds in the mLRSM being addressed in section 2.4). Furthermore, for a fixed value of the W_R-boson mass, the cross section value depends on the mass splitting between the W_R and N_R states. It hence decreases with decreasing values of $\Delta \equiv M_{W_R} - M_{N_R}$, as expected from the reduced phase space available for the decay when the two masses are similar. We also recall that cross sections for the electron and muon channels are identical, as predicted by the universality of the $\text{SU}(2)_R$ gauge coupling in the Lagrangian of eq. (2.4). Finally, K-factors are modest for most of the mass regime considered (i.e. for $M_{W_R} < 5$ TeV), and they lie between 1.1 and 1.5. The lowest values correspond to lighter W_R boson mass configurations while the larger ones correspond to the heaviest setups considered. Such a result is typical of the DY-like production of extra gauge bosons with masses in the TeV range, recalling that the behaviour of the K-factor is mostly independent of how the central scale is chosen [83, 86]. The K-factor however further increases to up to 3.3 for heavier W_R bosons with masses above 5 TeV, that also correspond to a regime in which PDF uncertainties are much larger and yield larger differences between LO predictions (involving a LO set of parton densities often associated with a poorer fit to data) and NLO predictions (involving an NLO set of parton densities).

2.4 Searches for W_R bosons in events with two leptons and two jets

In the previous sections, we mentioned the potential bounds that could be extracted from the first of the processes shown in eq. (2.9) and the associated searches at the LHC. In this section, we study the consequences of such searches on the model. To this aim, we reinterpret the results of the CMS-EXO-20-002 search targeting final states comprising two leptons (i.e. electrons or muons) and two (light) jets, using data collected between 2016 and 2018 and corresponding to an integrated luminosity of 138 fb^{-1} [52]. However, instead of extracting constraints directly from the published experimental results, we undertake our own interpretation study. The reason is that in the initial analysis, the CMS collaboration simulated the signal at LO, used global K-factors (as computed in section 2.3), and followed the prescription of refs. [59, 87]. Instead, we perform a more precise signal simulation at NLO in QCD, including real and virtual contributions to $\mathcal{O}(\alpha_s)$ at the fully differential level, and we additionally rely on more recent PDF sets. Our reinterpretation study however ignores any potential correlation between the different signal regions of the analysis, as relevant information has not been released by the CMS collaboration. In light of our findings and the experimental results published, we however do not expect that this issue would yield any significant change in our conclusions.
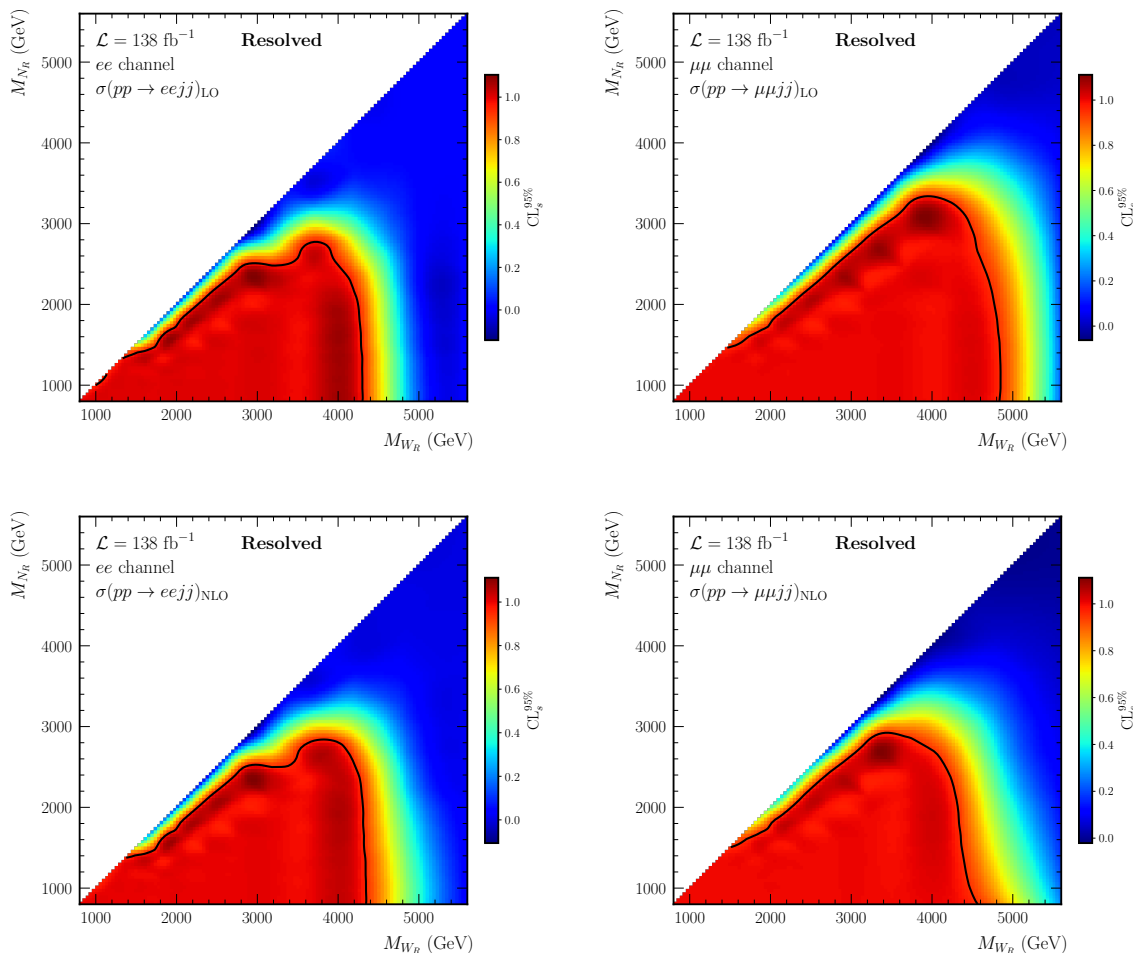
	Electron channel		Muon channel	
$]M_{\ell\ell jj}^{\min}, M_{\ell\ell jj}^{\max}]$	Data	Background	Data	Background
$]800, 1000]$ GeV	1106.0	1103.5 ± 26.607	1639.0	1670.7 ± 39.774
$]1000, 1200]$ GeV	646.0	631.51 ± 16.968	946.0	925.99 ± 23.917
$]1200, 1400]$ GeV	332.0	323.23 ± 10.736	518.0	500.33 ± 14.869
$]1400, 1600]$ GeV	170.0	169.69 ± 6.8418	268.0	263.88 ± 9.3498
$]1600, 2000]$ GeV	143.0	157.55 ± 9.505	216.0	215.18 ± 8.2146
$]2000, 2400]$ GeV	62.0	52.327 ± 3.9676	80.0	73.482 ± 4.4654
$]2400, 2800]$ GeV	25.0	19.567 ± 1.5493	30.0	25.943 ± 2.3125
$]2800, 3200]$ GeV	10.0	8.9907 ± 1.209	13.0	9.7557 ± 1.1603
$]3200, 8000]$ GeV	13.0	6.2463 ± 0.77892	11.0	7.8119 ± 0.84286

Table 1. Definition of the 18 signal regions of the CMS-EXO-20-002 search for W_R-boson production and decay in the $\ell\ell jj$ channel [52]. After a common pre-selection (see the description in the text), the different regions are defined according to the lepton flavour (electron or muon) and the value of the reconstructed W_R-boson mass $M_{\ell\ell jj}$. For each region, we show the number of observed events and the associated SM expectation.

The CMS-EXO-20-002 search is dedicated to the analysis of events featuring exactly two isolated leptons (electrons or muons, regardless of their electric charge), and at least two jets reconstructed by means of the anti-k_T algorithm [88, 89] with a radius parameter fixed to $R = 0.4$. For events exhibiting more than two jets, the two leading jets in terms of transverse momentum are considered to originate from the decay of a W_R boson, together with the two leptons. The leading and sub-leading charged leptons are required to have transverse momenta $p_T > 60$ and 53 GeV respectively, and to be within the detector acceptance (i.e. with a pseudo-rapidity $|\eta| < 2.4$, excluding electrons and positrons with a pseudo-rapidity lying in the interval $1.44 < |\eta| < 1.57$ that corresponds to the transition region between the barrel and endcap of the CMS electromagnetic calorimeter). Furthermore, selected jets must have a transverse momentum $p_T > 40$ GeV and pseudo-rapidity $|\eta| < 2.4$, the invariant mass of the reconstructed W_R-boson candidate is enforced to verify $M_{\ell\ell jj} > 800$ GeV, and the invariant mass of the lepton pair is constrained to fulfill $M_{\ell\ell} > 400$ GeV. After this pre-selection, the analysis defines 18 signal regions, 9 in the $eejj$ channel and 9 in the $\mu\mu jj$ channel, the various regions corresponding in different bins in $M_{\ell\ell jj}$. We report the exact definition of these bins, together with their background expectations and the associated observations, in table 1.

In order to determine the constraints that could be imposed on the mLRSM from LHC searches for W_R signatures in the $\ell\ell jj$ channel, we have implemented the CMS-EXO-20-002 search in the MADANALYSIS 5 framework [90–92]. Our implementation relies on the SFS module for the simulation of the detector effects via a parametrisation through transfer functions [93, 94], and it has been thoroughly validated by ensuring an excellent agreement with predictions provided by the CMS collaboration on HEPDATA [95]. Details on our implementation and its validation can be found in appendix A, as well as on the Public Analysis Database (PAD) [96] and the dataverse [97] of MADANALYSIS 5. In addition, we also provide in this appendix information on the implementation and validation of the superseded

Figure 3. Exclusion contours extracted from the reinterpretation of the results of the CMS-EXO-20-002 analysis, projected on the plane (M_{W_R}, M_{N_R}) in the electron (left) and muon (right) channel, when using matrix elements calculated at LO (top row) and NLO (bottom row). The black solid line corresponds to a CL_s value of $1 - CL_s = 0.95$, all mass points localised on its lower left being thus excluded.

CMS-EXO-17-011 search dedicated to the same signal, but in which only a partial LHC Run 2 dataset is analysed. This older search had been initially used for the present work, until the more recent CMS-EXO-20-002 results appeared.

The resulting constraints on the model are derived from a scan of the two-dimensional plane defined by the masses M_{W_R} and M_{N_R}, which we vary in the range [800, 5300] GeV. We analysed 120 signal configurations with $M_{N_R} \leq M_{W_R}$, generating 500,000 hard-scattering events for each. Subsequently, we utilised PYTHIA version 8.309 [98] for simulating parton showering and hadronisation. The resulting hadron-level events were then analysed with MADANALYSIS 5, employing the CL_s method [99] to assess the signal's viability with respect to data. We report the obtained CL_s values in figure 3, both for the electron (left) and muon (right) channels and using LO (top row) and NLO (bottom row) simulations. We obtain in general results in the same ballpark as those presented officially in the CMS analysis [52], demonstrating hence by different means the validity of our implementation of the CMS analysis in our tool chain.
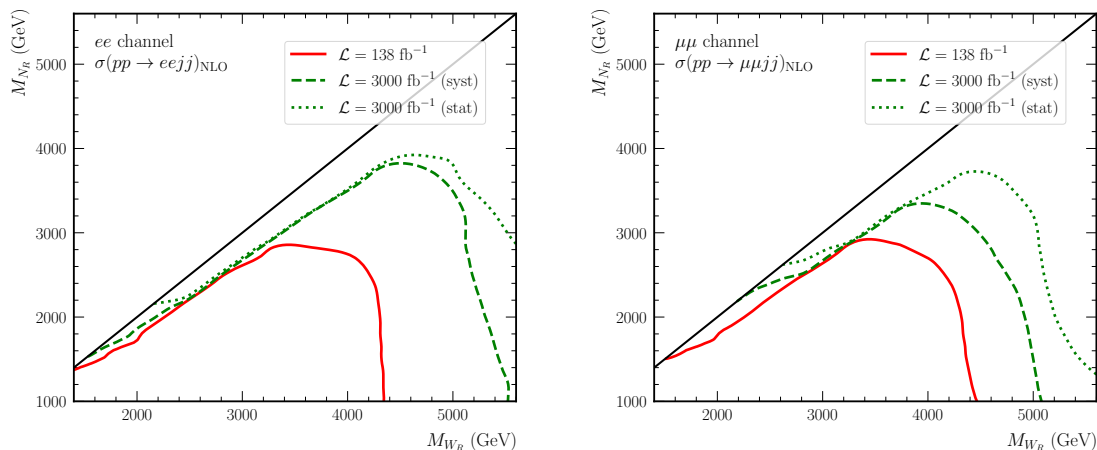
Figure 4. Exclusion contours in the plane (M_{W_R}, M_{N_R}) as obtained from the recasting of the CMS-EXO-20-002 search in the $eejj$ (left) and $\mu\mu jj$ (right) channel, from NLO signal simulations. We compare current exclusions (solid red) to expectations at the high-luminosity LHC with $3000\,\mathrm{fb}^{-1}$, assuming that the background uncertainties are dominated by the statistical (dotted green) or systematic (dashed green) components.

In the electron channel, we exclude W_R bosons with masses smaller than $4.3\,\mathrm{TeV}$, given that the mass splitting Δ between the W_R boson and the right-handed neutrino N_R is significant. In the most extreme situation featuring a W_R boson of 4–$5\,\mathrm{TeV}$, N_R masses ranging up to 3–$3.2\,\mathrm{TeV}$ can be reached. The CMS official bounds are, in comparison, slightly stronger by about 1-2σ. This difference is mitigated when comparing our NLO exclusions to the CMS official ones, which are based on LO simulations including an NLO K-factor. In this case, the remaining difference is less than 10% when considering the mass limit values, as expected due to the entirely different nature of the detector simulations employed in this work (the SFS framework) and in the CMS analysis (the CMS simulation software based on GEANT 4).

Results in the muonic channel are more intriguing. Similar to the electronic case, our LO limits are in the same ballpark as the CMS official ones, with the latter being slightly stronger. However, with NLO simulations we observe a decrease in sensitivity predicted by MADANALYSIS 5. It is important to note that the limits found lie close to the regime where the K-factors displayed in figure 2 are larger than 2, in contradiction with naive expectations of a DY-like process. This behaviour can be traced back to the impact of the differences between the poor LO and the better NLO NNPDF 4.0 parton density fits, which therefore significantly modify not only total rates but also event kinematics. As NLO PDF fits are better than LO fits, we rely on NLO simulations only from now on.

We close this section by estimating the change in the exclusion contours when the LHC luminosity is scaled to $\mathcal{L} = 3000\ \mathrm{fb}^{-1}$, which corresponds to the high-luminosity LHC phase. We assume the same search strategy as in [52], and naively re-scale the exclusion contours following the methods presented in ref. [100]. We consider that the expected number of background events for each signal region, shown in table 1, scales proportionally to the luminosity, and that the scaling of the uncertainties on the background is achieved in two different complementary ways depending on whether background errors are dominated by statistical uncertainties or by systematic ones. We consider the two cases, and derive expected

limits by assuming observations in agreement with the SM background. The results are displayed in figure 4. They show that W_R-boson masses between 5 and 6 TeV can be reached, together with right-handed neutrino masses ranging up to 4 TeV.

3 Sensitivity of $\ell\ell tb$ probes to left-right models

In section 2, we focused on existing LHC searches for mLRSM signals in which a W_R boson decays into a lepton pair and a di-jet system. However, for heavier spectra, decays into a lepton pair and a top-bottom system could as well contribute. We therefore focus in this section on the second process of eq. (2.9), illustrated by the second diagram in figure 1. In order to assess the potential of the LHC to such a signal, we consider a set of benchmark scenarios that satisfy all current constraints, and then design a dedicated phenomenological analysis that could potentially seed future experimental searches in proton-proton collisions at a centre-of-mass energy of $\sqrt{s} = 13.6$ TeV.

3.1 Benchmark scenarios and backgrounds

In order to build our analysis, we define Benchmark Points (BPs) that fulfill all constraints from searches for W_R bosons in the $\ell\ell jj$ channel presented in the previous section. We consider two mass values for a W_R boson decaying in the di-electron channel ($W_R \to eetb$), namely $M_{W_R} = 4800$ and 5500 GeV, and two mass values for the di-muon channel ($W_R \to \mu\mu tb$), namely $M_{W_R} = 5100$ and 5500 GeV. For each of these mass values, we then define three scenarios differing by the choice of the right-handed neutrino mass,

$$M_{N_R} \in \left\{ \frac{M_{W_R}}{5}, \ \frac{M_{W_R}}{2}, \ M_{W_R} - 400 \ \text{GeV} \right\}.$$

Such a choice allows us to span most of the possible kinematic configurations in terms of the splitting $\Delta \equiv M_{W_R} - M_{N_R}$. The definitions of these different BPs are collected in table 2 for both the electron channel (upper part of the table) and the muon channel (lower part of the table), and we also indicate some of the properties of these scenarios relevant for the signal.

In order to extract the mLRSM signal from the SM background, we focus on hadronic top quark decays so that the final state considered comprises exactly two charged leptons, and several jets whose hardness and multiplicity depend on the kinematic properties of the signal. For relatively small top quark transverse momenta (typically smaller than 500 GeV), events generally feature at least four small-radius jets, while for larger top quark transverse momenta we should have at least one large-R jet and at least one small-R jet. The lowest N_R mass chosen for the scenarios explored in our study being fixed to 960 GeV (BP$e1$), the produced top quarks have typically very high transverse momenta in most of the targeted cases. mLRSM spectra yielding softer top quarks are indeed already challenged by existing data and thus hard to justify phenomenologically. The backgrounds associated to our signal process thus usually emerge from the production of high-p_T top quarks, with a much smaller contribution originating from the production of two massive gauge bosons in association with jets that we therefore do not consider. The list of all background contributions is given in table 3, together with the related LO and NLO cross sections.

BP	BPe1	BPe2	BPe3
M_{W_R} [GeV]	4800	4800	4800
M_{N_R} [GeV]	960	2400	4400
$\sigma(pp \to \ell\ell tb)_{\rm LO}$ [fb]	1.22×10^{-1}	7.77×10^{-2}	4.27×10^{-3}
$\sigma(pp \to \ell\ell tb)_{\rm NLO}$ [fb]	1.73×10^{-1}	1.13×10^{-1}	6.43×10^{-3}
Γ_{W_R} [GeV]	134	130	122
Γ_{N_R} [GeV]	2.47×10^{-5}	2.96×10^{-3}	1.21×10^{-1}

BP	BPe4	BPe5	BPe6
M_{W_R} [GeV]	5500	5500	5500
M_{N_R} [GeV]	1100	2750	5100
$\sigma(pp \to \ell\ell tb)_{\rm LO}$ [fb]	3.39×10^{-2}	1.73×10^{-2}	6.87×10^{-4}
$\sigma(pp \to \ell\ell tb)_{\rm NLO}$ [fb]	5.50×10^{-2}	3.13×10^{-2}	1.34×10^{-3}
Γ_{W_R} [GeV]	153	149	139
Γ_{N_R} [GeV]	2.88×10^{-5}	3.41×10^{-3}	1.52×10^{-1}

BP	BPμ1	BPμ2	BPμ3
M_{W_R} [GeV]	5100	5100	5100
M_{N_R} [GeV]	1020	2550	4700
$\sigma(pp \to \ell\ell tb)$ [fb]	6.99×10^{-2}	4.09×10^{-2}	1.54×10^{-3}
$\sigma(pp \to \ell\ell tb)_{\rm NLO}$ [fb]	1.04×10^{-1}	6.45×10^{-2}	3.25×10^{-3}
Γ_{W_R} [GeV]	142	138	129
Γ_{N_R} [GeV]	2.65×10^{-5}	3.15×10^{-3}	1.34×10^{-1}

BP	BPμ4	BPμ5	BPμ6
M_{W_R} [GeV]	5500	5500	5500
M_{N_R} [GeV]	1100	2750	5100
$\sigma(pp \to \ell\ell tb)_{\rm LO}$ [fb]	3.39×10^{-2}	1.73×10^{-2}	6.87×10^{-4}
$\sigma(pp \to \ell\ell tb)_{\rm NLO}$ [fb]	5.50×10^{-2}	3.13×10^{-2}	1.34×10^{-3}
Γ_{W_R} [GeV]	153	149	139
Γ_{N_R} [GeV]	2.88×10^{-5}	3.41×10^{-3}	1.52×10^{-1}

Table 2. Definition of the 12 BPs used in our analysis, for W_R decays into a $eetb$ system (BPe1 to BPe6) and $\mu\mu tb$ system (BPμ1 to BPμ6). These benchmarks satisfy current constraints originating from W_R production and decay into an $\ell\ell jj$ final state, and they feature a variety of split and more compressed spectra. For each scenario, we additionally report LO and NLO signal cross sections at $\sqrt{s} = 13.6\,{\rm TeV}$, as well as the total decay widths of the W_R and N_R states.

Process	σ_{LO} [fb]	σ_{NLO} [fb]	$K \equiv \sigma_{\mathrm{NLO}}/\sigma_{\mathrm{LO}}$	N_{events}
$pp \to t\,\bar{t}\,H$	345.5	503.8	1.45	1.6×10^6
$pp \to t\,\bar{t}\,Z$	519.1	838.9	1.61	1.6×10^6
$pp \to t\,\bar{t}\,W^{\pm}$	434.0	670.2	1.54	1.6×10^6
$pp \to t\,Zj + \mathrm{c.c.}$ [101]	821.4	903.5	1.10	2.2×10^6
$pp \to t\,W^-\bar{b} + \mathrm{c.c.}$ [102]	976.4	1331.5	1.36	4.0×10^6

Table 3. Total cross sections at $\sqrt{s} = 13.6\,\mathrm{TeV}$ for all background processes relevant to our study, shown both at LO and NLO, along with the corresponding K-factor and the number of generated events. Here, $\sigma_{tZj} \equiv \sigma(pp \to tZj) \times \mathrm{BR}(t \to bjj) \times \mathrm{BR}(Z \to \ell^+\ell^-)$ and $\sigma_{tWb} \equiv \sigma(pp \to tWb) \times \mathrm{BR}(t \to b\ell\nu) \times \mathrm{BR}(W \to \ell\nu)$. Total rate predictions have been obtained with MadGraph5_aMC@NLO, unless indicated otherwise through a reference.

$M_{\ell\ell tb}$ \ $M_{\ell\ell}$	$]400, \infty)$	$]600, \infty)$	$]800, \infty)$
$]1200, \infty)$	SRa1	SRb1	SRc1
$]1400, \infty)$	SRa2	SRb2	SRc2
$]1600, \infty)$	SRa3	SRb3	SRc3
$]1800, \infty)$	SRa4	SRb4	SRc4
$]2000, \infty)$	SRa5	SRb5	SRc5
$]2500, \infty)$	SRa6	SRb6	SRc6
$]3000, \infty)$	SRa7	SRb7	SRc7

Table 4. Definitions of the SRs of our analysis in terms of bins in the invariant mass of the reconstructed W_R boson $M_{\ell\ell tb}$ and the invariant mass of the lepton pair $M_{\ell\ell}$.

Background event generation and cross section calculations have been achieved with the same tool chain as the one described in section 2.3, with the exception of the NLO total cross sections relevant to single top production in association with a Z boson or a W boson that we extracted from refs. [101] and [102] respectively. Detector simulation relies on the SFS framework with a detector parametrisation matching the one that we used for the implementation of the CMS-EXO-20-002 search in MadAnalysis 5 (see appendix A for more details), with the exception of the b-tagging efficiency that we take equal to 70%. Event reconstruction relies on the definition of two jet collections. The first one includes small-R 'AK04' jets clustered using the anti-k_T algorithm and a jet radius parameter of $R = 0.4$, while the second one comprises large-R 'CA15' jets clustered using the Cambridge-Aachen algorithm [103, 104] with a radius parameter of $R = 1.5$. Finally, boosted top quark candidates are reconstructed by means of HepTopTagger [105, 106], as integrated within the jet substructure module of MadAnalysis 5 [107].

3.2 Description of the analysis

Events are selected if they contain exactly two isolated electrons or muons with $p_T > 25\,\mathrm{GeV}$ for electrons and $p_T > 33\,\mathrm{GeV}$ for muons, and $|\eta| < 2.4$ in both cases. Moreover, we
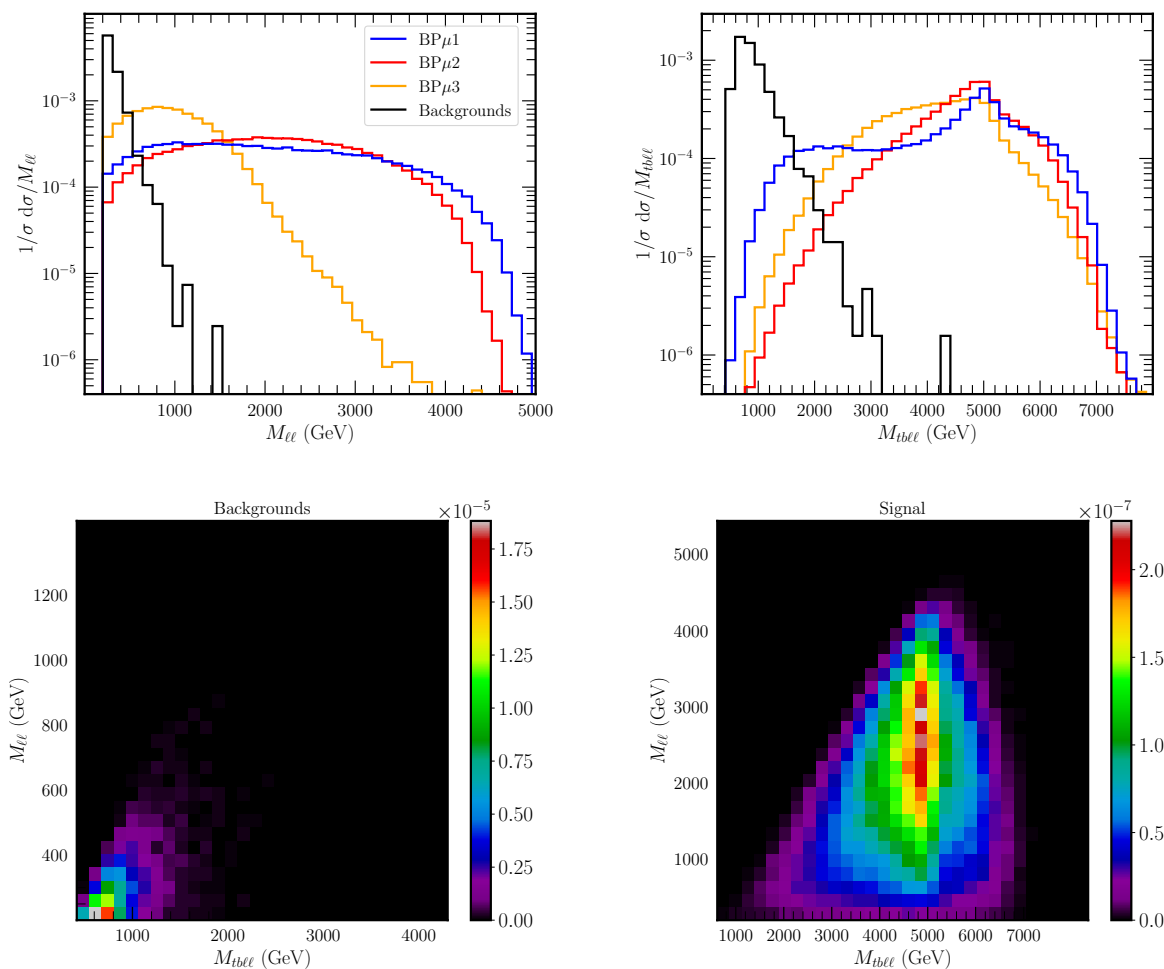
Figure 5. Normalised distributions in the invariant mass of the di-lepton system $M_{\ell\ell}$ (top left) and of the reconstructed W_R boson $M_{\ell\ell tb}$ (top right) after the selection described in the text, both for the background (solid black) and the three representative signal scenarios BPμ1 (blue), BPμ2 (red) and BPμ3 (orange). We additionally display the correlations between these two variables, both for the background (bottom left) and the BPμ2 signal (bottom right). The colour code refers to a total number of entries in the maps, normalised to unity.

remind that lepton isolation is encoded directly in our SFS detector parametrisation. The leading and sub-leading charged leptons are next enforced to satisfy $p_T > 60\,\mathrm{GeV}$ and $p_T > 53\,\mathrm{GeV}$ respectively, and we veto events featuring hadronically decaying tau-leptons with $p_T > 30\,\mathrm{GeV}$ and $|\eta| < 2.5$. We then select events that contain at least one AK04 b-tagged jet with $p_T > 30\,\mathrm{GeV}$ and $|\eta| < 2.5$, and at least one top-tagged CA15 jet with $p_T > 200\,\mathrm{GeV}$, $|\eta| < 2$, and an invariant mass $M_{\mathrm{HTT}} \in\,]145, 210[\,\mathrm{GeV}$. Finally, we require that the invariant mass of the two charged leptons satisfies $M_{\ell\ell} > 200\,\mathrm{GeV}$. The resulting selection efficiency is 6.67×10^{-4} and 1.54×10^{-3} for the $t + X$ and $t\bar{t} + X$ components of the background, respectively. On the other hand, for the signal processes the accumulated efficiency varies between 2.9% and 5.4% for the electron channel and between 14% and 18% for the muon channel, the higher efficiencies corresponding to scenarios with larger right-handed

neutrino masses. Moreover, the higher prospects for the muon channel are directly related to the higher reconstructed efficiencies for high-p_T muons than for corresponding electrons.

To improve signal significance we define several signal regions (SRs) targeting different bins in the invariant masses of the di-lepton system ($M_{\ell\ell}$) and of the reconstructed W_R boson candidate ($M_{\ell\ell tb}$). To better understand this choice of variables, we display in figure 5 (top row) the associated normalised distributions for the background and a selection of three illustrative signal benchmark points (BPμ1, BPμ2 and BPμ3), after imposing the selection $M_{\ell\ell} > 200\,\text{GeV}$. The resonant contributions specific to the signal leads to very hard distributions exhibiting a very broad plateau (or peak), deep in the multi-TeV regime. This contrasts with the SM background, that exhibits a steeply falling spectrum with very few events expected for invariant masses larger than 1 TeV for the $M_{\ell\ell}$ spectrum or 2–3 TeV for the $M_{\ell\ell tb}$ one. The same information is displayed jointly through the correlations between these two variables in the bottom row of the figure, in which we focus on the background (bottom left) and the illustrative BPμ2 scenario (bottom right). We subsequently define 21 SRs in each of the electron and muon channels as shown in table 4.

3.3 Results

In figure 6 we display the number of events populating the different signal regions of our analysis, both for the signal process in the case of the 12 benchmark points considered and the different contributions to the background. We collectively group the latter into a single top component (orange) and $t\bar{t}$ pair component (kaki), and we show results both for the electron channel (upper panel) and muon channel (lower panel). As already mentioned in section 3.1, events are normalised to their total rates at NLO in the strong coupling. It is immediate to see that there is a high discovery potential for the signal, specifically in the muon channel. This originates from the fact that our analysis comprises some SRs that are essentially background-free, and that turn out to be the SRs dedicated to scenarios with heavy W_R bosons.

In order to assess the sensitivity of the LHC to the signal process considered as a function of the integrated luminosity, we extract the CL_s exclusion and associated 1σ and 2σ bands for the best expected signal region (SRb7), by means of the package PYHF [108]. Whereas more aggressive estimates could be obtained by combining the different signal regions of the analysis, we refrain from doing so in order to get predictions as conservative as possible. Our goal is indeed to demonstrate that for scenarios not excluded by analyses of the $\ell\ell jj$ signature of W_R-boson production and decay, there is a potential gain in studying the corresponding third-generation signal $\ell\ell tb$. Our calculation relies on several assumptions. First, we conservatively assume that there is at least one background event regardless of the luminosity. Consequently, we always fix the number of background event to $n_b = 1$ for signal regions in which our simulations yield $n_b < 1$. Next, we assume that there is a systematic uncertainty of 20% on the background yields. Finally, we estimate that the number of events to be observed is always equal to those predicted in the context of the SM.

The results are shown in figure 7 for the electron (upper panel) and muon (lower panel) channels. For the electron channel, it is clear that a large luminosity is required in order to probe the model. A few ab^{-1} are indeed necessary to exploit the small signal cross sections
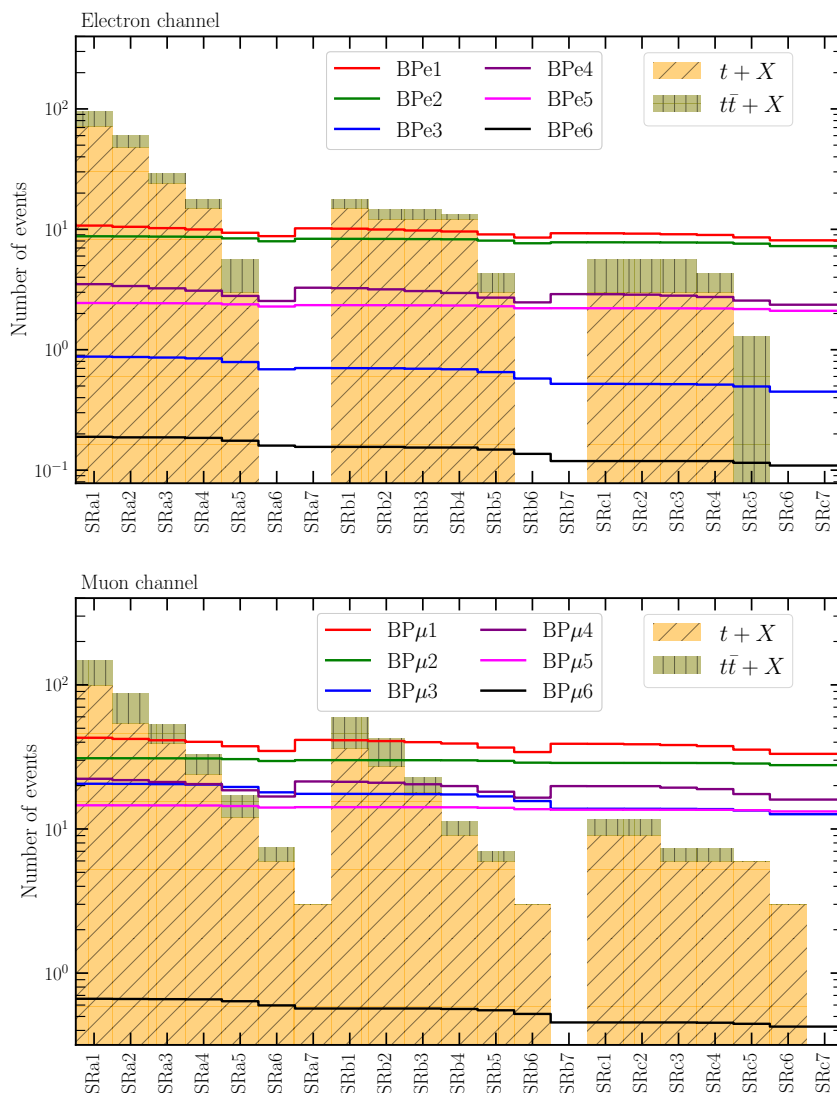
Figure 6. Number of background and signal events populating the different SRs in the electron (upper) and muon (lower) channels, for $\mathcal{L} = 3000\,\text{fb}^{-1}$. Our predictions are normalised to NLO in QCD, and we collect the background contributions into a single top contribution (orange) and top-antitop contribution (kaki). Signal predictions are made for the 12 BPs considered (solid lines).

(see table 2). Consequently, only benchmarks for which the W_R boson is not too heavy and in which the new physics spectrum is not too compressed could yield some sensitivity. We find that it is indeed the case, as shown by the predictions made in the upper panel of the figure. Only the two first scenarios, BPe1 and BPe2, have the potential to be excluded at 95% confidence level, and this can only be achieved around the ultimate end of the high-luminosity LHC runs. In contrast, results in the muon channel are more promising, by virtue of the larger reconstruction efficiencies for high-p_T muons than for electrons. More of our selected benchmarks are found reachable, and this for a smaller integrated luminosity (of about 1 ab^{-1}) than in the electron channel. All muonic scenarios with the exception of BPμ6 are hence potentially observable, and it becomes clear that charged gauge boson masses ranging
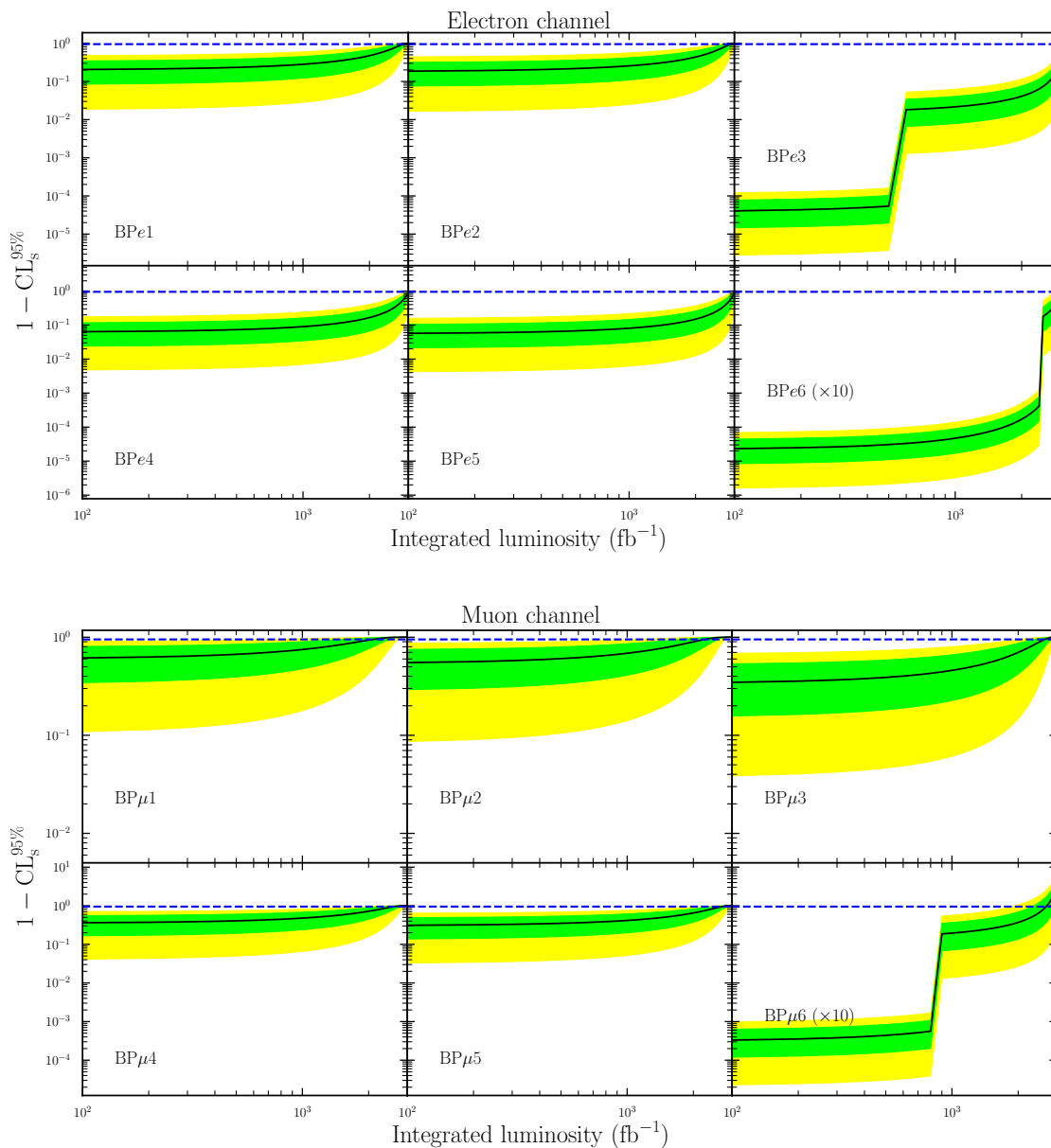
Figure 7. Evolution of the exclusion CL_s as a function of the luminosity for the electron (upper) and muon (lower) channels, for each of the BPs considered. The central values are depicted through a solid black line, together with the associated 1σ (lime) and 2σ (yellow) bands. The horizontal blue dashed line corresponds to $\mathrm{CL}_\mathrm{s} = 0.95$, above which the parameter point is excluded at 95% confidence level.
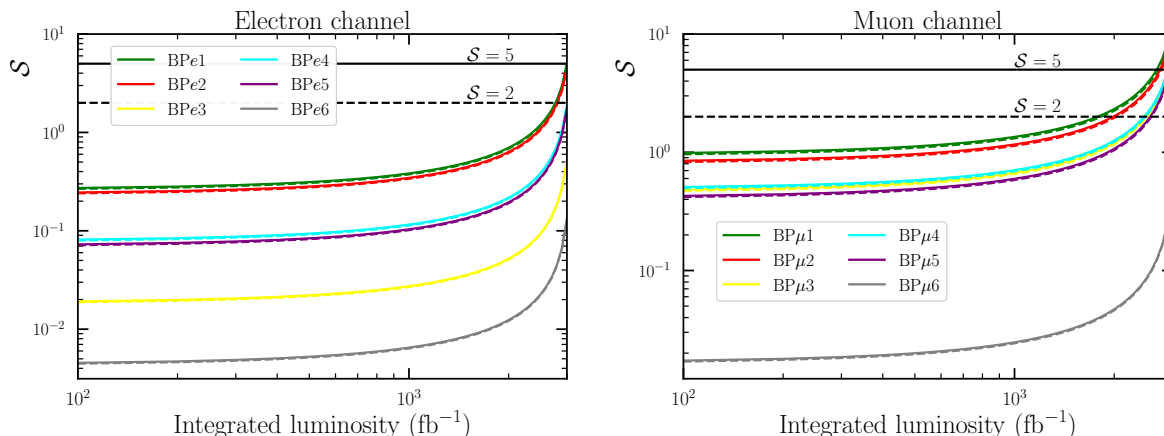
Figure 8. Signal significance $\mathcal{S}$ for the electron (left) and muon (right) channels. Results are shown for the scenarios BP$\ell 1$ (green), BP$\ell 2$ (red), BP$\ell 3$ (yellow), BP$\ell 4$ (cyan), BP$\ell 5$ (purple) and BP$\ell 6$ (gray) and for two choices of background uncertainties: the ideal case in which there is no error on the background (solid lines), and a more realistic situation embedding a level of systematics equal to 20%. The horizontal dashed and solid black lines correspond to the exclusion and discovery limits for which $\mathcal{S} = 1$ and $\mathcal{S} = 5$ respectively.

up to at least $W_R = 5.5$ TeV could be probed during the high-luminosity phase of the LHC, provided that the mass splitting between the W_R boson and the right-handed heavy neutrino N_R is not too small. The $\ell\ell tb$ channel has thus a strong potential as a probe to left-right models, similar to the $\ell\ell jj$ channel (see figure 4).

In figure 8, we illustrate these results in a complementary way through the calculation of the signal significance $\mathcal{S}$ as a function of the integrated luminosity, both for the electron (left panel) and muon (right panel) channel. Using the formulas introduced in ref. [109], we make use of

$$\mathcal{S} = \sqrt{2} \left[(n_s + n_b) \log \left(\frac{(n_s + n_b)(n_b + \delta_b^2)}{n_b^2 + (n_s + n_b)\delta_b^2} \right) - \frac{n_b^2}{\delta_b^2} \log \left(1 + \frac{\delta_b^2 n_s}{n_b(n_b + \delta_b^2)} \right) \right]^{1/2}, \qquad (3.1)$$

where n_s and n_b are the number of signal and background events, and where the systematic error on the background $\delta_b = x n_b$. We use the same error configuration as above, and we thus assume that $x = 0.20$ and that n_b is of at least 1 (dashed lines). For informative purposes, we additionally consider the ideal case of $x = 0$ (solid lines). This consistently confirms that the two electron scenarios BP$e1$ and BP$e2$ can be reached at the high-luminosity LHC, and this for luminosities around 2.5 ab^{-1}, and that the first five muonic BPs can be probed with luminosities of $\mathcal{O}(1)$ ab^{-1}.

We close this section by discussing briefly the capability of our search strategy to disentangle between the different BPs, i.e. by assessing the value of the right-handed neutrino mass. In our analysis we did not make use of the reconstructed N_R mass, defined as the invariant mass of the $tb\ell$ system, for the reason that we wanted to optimise the signal-to-background ratio with minimal model assumptions. However, the determination of the N_R mass can always be achieved post-discovery. In the production channel considered, the charged lepton that is emerging from the decay of the right-handed neutrino N_R, along with
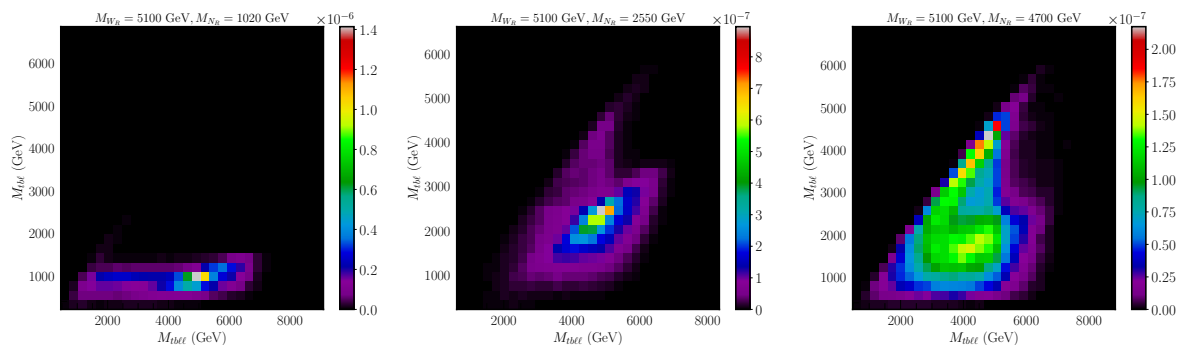
Figure 9. 2D correlations between $M_{\ell\ell tb}$ and $M_{\ell tb}$ for the signal for BPμ1 (left upper panel), BPμ2 (right upper panel) and BPμ3 (lower panel). The colour code corresponds to the number of entries normalised to unit integral.

the top and bottom jets, can be tagged using a ΔR requirement: the N_R candidate comprises the lepton with the minimal separation from the top-bottom system. As an example, we display in figure 9 correlation maps relating the invariant mass of the W_R system ($M_{\ell\ell tb}$) and the one of the N_R candidate ($M_{\ell tb}$), for the three most optimistic scenarios BPμ1 (left panel), BPμ2 (central panel) and BPμ3 (right panel). These scenarios all feature the same W_R boson mass, $M_{W_R} = 5.1$ TeV, but they differ with the chosen value of the right-handed neutrino mass so that different level of spectrum compression are considered. Predictions are presented for the signal region SRb7, that is essentially background-free and dedicated to scenarios with very large W_R-boson mass. This region corresponds to a mass window reasonably populated, which ensures good statistics for the signal ($n_s \approx 10$–40 events). Our results therefore demonstrate that our simple analysis has an intrinsic ability to identify the underlying mLRSM scenario.

4 Conclusions

We have proposed a novel search channel for $SU(2)_R$ charged gauge bosons typical of left-right symmetric models, which exploits the fact that such bosons often decay, via right-handed neutrinos, into a final state made of a highly-boosted top quark, a b-jet and two charged leptons. This new avenue supplements traditional analyses that exploit the $\ell\ell jj$ signature, where j represents a light jet. After discussing in detail the effects of existing searches on the viability of scenarios featuring a W_R boson and a right-handed neutrino N_R in a minimal left-right configuration, we have defined a few phenomenologically-viable scenarios that could be tested at future runs of the LHC. We have analysed the properties of W_R and N_R production and decay in these benchmark scenarios, and we have then built a new analysis strategy relying on the richness of the $\ell\ell tb$ final state. We have in particular made use of two kinematic variables to enhance the signal-to-background ratio, namely, the invariant masses of the di-lepton system ($M_{\ell\ell}$) and that of the W_R-boson candidate ($M_{\ell\ell tb}$). These variables have allowed for the definition of different SRs targeting different mLRSM spectra in terms of mass scale and regime of compression, guaranteeing hence in a very significant way a potential observation of the signal above the background.

Our results demonstrated that analyses of the $\ell\ell tb$ channel could probe left-right models as well as analyses relying on the $\ell\ell jj$ channel. We have shown that, in the electron mode ($eetb$), scenarios featuring a W_R-boson with mass ranging up to 4.8 TeV and a right-handed neutrino N_R with mass lying between $M_{W_R}/5$ and $M_{W_R}/2$, have the potential to be probed during the high-luminosity phase of the LHC. Furthermore, in the muon channel ($\mu\mu tb$), W_R-boson masses ranging up to 5.5 TeV can be reached for N_R masses lying between $M_{W_R}/5$ and $M_{W_R}/2$, although M_{N_R} can also sometimes be even larger. In addition, our approach is beneficial when it comes to profiling the underlining new physics scenario, as N_R reconstruction is also possible. This in turn enables new physics characterisation through the exploitation of all information available from the rich final state inherent to $\ell\ell tb$ production via W_R and N_R exchanges, by virtue of the combination of W_R and N_R reconstruction.

The method that we proposed in this work can be improved further. First, better electron and muon identification efficiencies could increase fiducial signal rates, which would subsequently increase the sensitivity reach. This is especially crucial for the electron channel where lower reconstruction and identification efficiencies are currently in order. Second, one could use more sophisticated jet substructure techniques that will allow for the definition of the whole N_R candidate as a single large R-jet with some specific substructure properties. Consequently, heavy-neutrino jets could be distinguished from more regular top-quark, W-boson, Z-boson or Higgs-boson jets. Such methods targeting jets with more than three prongs belong however to an uncharted territory, as far as we know, and they will need to be studied comprehensively. Third, we expect that machine-learning techniques could impact the signal significance very positively, and improve both large-R jet identification and cut-flow optimisation. Finally, we remark that a simple search strategy, similar to the one that we proposed in this work, could also be used to probe lepton-flavour-violating or lepton-number-violating W_R-boson decays. All these items should however preferably be addressed in the context of an experimental search. We therefore urge the experimental collaborations at the LHC to carry out a search for W_R bosons and right-handed neutrinos N_R as we proposed.

A   Reinterpretation of CMS searches for W_R bosons with leptons and jets

In this section, we present details about predictions obtained with in-house implementations, in the MADANALYSIS 5 framework [90–92], of two CMS searches for $SU(2)_R$ gauge bosons and right-handed neutrinos in final states comprising two charged leptons (electrons or muons) and at least two jets. We consider LHC run 2 searches at $\sqrt{s} = 13$ TeV that focus on integrated luminosities of 35.9 fb^{-1} [50] and 138 fb^{-1} [52]. We have validated these

implementations by comparing cut-flows predicted with our tool chain to official results provided by the CMS collaboration for well-defined benchmark scenarios. The corresponding codes and the validation material is public, integrated in MADANALYSIS 5, and can be found on the software dataverse [97, 110]. In the following, we first discuss generalities common to the two implemented analyses in section A.1, and we next detail the validation of the two implementations in sections A.2 and A.3.

A.1 Object definitions and detector modeling

The signal topology is such that the two produced final-state leptons carry a large fraction of the $SU(2)_R$ gauge boson energy. The two CMS analyses considered exploit this, and they consequently rely on triggers on leptons with very high transverse momentum to optimise signal efficiency. In CMS-EXO-17-011, the electron channel relies on a double-electron trigger that requires that the event final state features at least two electrons with a transverse momentum $p_T > 33$ GeV and associated to important deposits in the electromagnetic calorimeter. For the muon channel, a single-muon trigger is used instead, which requires the presence of at least one muon with $p_T > 50$ GeV. In its more recent CMS-EXO-20-002 search, the CMS collaboration improves electron triggering through a combination of three triggers. The event final state must exhibit the presence of at least either an isolated electron with $p_T > 27$ (32) GeV, an electron with $p_T > 115$ GeV, or a photon with $p_T > 175$ (200) GeV for the 2016 (2018) dataset.

As in all CMS searches, event reconstruction is performed by means of the particle-flow algorithm [111]. We briefly summarise below object identification requirements used in the two CMS searches considered, and we refer interested readers to refs. [50, 52] for more details.

- Electron candidates are identified by associating charged-particle tracks from the primary vertex with energy deposit clusters in the electromagnetic calorimeter.
- Muon candidates are identified by combining tracker and muon chamber information.
- Charged hadrons reconstruction involves the matching of tracks with calorimeter cells, together with the absence of any associated activity in the muon chamber.
- Neutral hadrons arises from the presence of clusters in both the electromagnetic and hadronic calorimeters and the absence of any associated charged particle track.
- Jets are defined from the clustering of reconstructed particles by means of the anti-k_T algorithm [88, 89] with a jet radius $R = 0.4$. Charged and neutral hadrons originating from pile-up interactions are removed through a dedicated pileup subtraction method [111] and residual average area-based corrections [112].

We model detector effects with the SFS module of MADANALYSIS 5 [93, 94]. Smearing and reconstruction efficiencies related to the different objects are tuned according to the CMS analyses considered, that we implement through approximate semi-analytical formulas. For energy and momentum smearing, we use the parametrisation included in the default CMS card shipped with MADANALYSIS 5 (see also refs. [113–116]). We then implement the following identification efficiencies for jets ($\mathcal{E}_j$), muons ($\mathcal{E}_\mu$) and electrons ($\mathcal{E}_e$):

$$\mathcal{E}_j = \begin{cases} 0.925 & \text{if } |\eta| \leq 1.5, \\ 0.875 & \text{if } 1.5 < |\eta| \leq 2.5, \\ 0.80 & \text{if } 2.5 < |\eta|. \end{cases} \tag{A.1}$$

Cut	Definition
Initial	Initial number of events corresponding to 35.9 fb^{-1}
$N_{\text{jets}} \geq 2$	At least two jets with $p_T > 25$ GeV and $|\eta| < 2.4$
$N_\ell \geq 2$	At least two isolated charged leptons
$p_T^j > 40$ GeV	The p_T of the two leading jets should be larger than 40 GeV
$p_T^{\ell_1} > 60$ GeV	The p_T of the leading lepton should be larger than 60 GeV
$p_T^{\ell_2} > 53$ GeV	The p_T of the sub-leading lepton should be larger than 53 GeV
$\Delta R_{\ell j} > 0.4$	Leptons and jets should be separated by at least $\Delta R > 0.4$
$M_{\ell\ell} > 200$ GeV	The di-lepton invariant mass should be larger than 200 GeV
$M_{\ell\ell jj} > 600$ GeV	The reconstructed W_R invariant mass should be larger than 600 GeV

Table 5. Definition of the different cuts used in the CMS–EXO–17–011 search [50].

$$
\mathcal{E}_e = \begin{cases}
0.00 & \text{for } p_T \leq 0.1 \text{ GeV}, \\
0.73 & \text{for } |\eta| \leq 1.5 \text{ and } p_T \in \,]0.1, 1] \text{ GeV}, \\
0.95 & \text{for } |\eta| \leq 1.5 \text{ and } p_T \in \,]1, 100] \text{ GeV}, \\
0.83 & \text{for } |\eta| \leq 1.5 \text{ and } p_T > 100 \text{ GeV}, \\
0.50 & \text{for } 1.5 < |\eta| \leq 2.5 \text{ and } p_T \in \,]0.1, 1] \text{ GeV}, \\
0.83 & \text{for } 1.5 < |\eta| \leq 2.5 \text{ and } p_T \in \,]1, 100] \text{ GeV}, \\
0.83 & \text{for } 1.5 < |\eta| \leq 2.5 \text{ and } p_T > 100 \text{ GeV}, \\
0.00 & \text{for } |\eta| > 2.5,
\end{cases} \tag{A.2}
$$

$$
\mathcal{E}_\mu = \begin{cases}
0.00 & \text{for } p_T \leq 0.1 \text{ GeV}, \\
0.75 & \text{for } |\eta| \leq 1.5 \text{ and } p_T \in \,]0.1, 1] \text{ GeV}, \\
0.99 & \text{for } |\eta| \leq 1.5 \text{ and } p_T \in \,]1, 100] \text{ GeV}, \\
0.99 \times \exp\{0.5 - 5 \times 10^{-4} \, p_T\} & \text{for } |\eta| \leq 1.5 \text{ and } p_T > 100 \text{ GeV}, \\
0.70 & \text{for } 1.5 < |\eta| \leq 2.5 \text{ and } p_T \in \,]0.1, 1] \text{ GeV}, \\
0.98 & \text{for } 1.5 < |\eta| \leq 2.5 \text{ and } p_T \in \,]1, 100] \text{ GeV}, \\
0.98 \times \exp\{0.5 - 5 \times 10^{-4} \, p_T\} & \text{for } 1.5 < |\eta| \leq 2.5 \text{ and } p_T > 100 \text{ GeV}, \\
0.00 & \text{for } |\eta| > 2.5,
\end{cases} \tag{A.3}
$$

A.2 CMS-EXO-17-011

The CMS-EXO-17-011 analysis is dedicated to events with at least two high-p_T leptons and two jets. The two leptons, together with the two jets with the largest p_T, are considered to originate from the decay of a W_R boson. The selection, that is described in table 5, first imposes that the leading and sub-leading leptons have transverse momentum $p_T > 60$ and 53 GeV respectively, and that they both lie within the detector acceptance ($|\eta| < 2.4$, with electrons being rejected if $1.444 < |\eta| < 1.566$). Muon isolation is enforced by imposing that the charged-track activity in a cone of $\Delta R = 0.3$ centred on the muon is of at most 10% of

	$M_{W_R} = 2200\,\text{GeV}$		$M_{W_R} = 2800\,\text{GeV}$		$M_{W_R} = 3600\,\text{GeV}$	
Electron channel	Events	ε	Events	ε	Events	ε
Initial	1507.8	–	366.2	–	58.9	–
$N_{\text{jets}} \geq 2$	1505.4 ± 0.6	0.998	365.5 ± 0.2	0.998	58.9 ± 0.0	0.999
$N_\ell \geq 2$	752.1 ± 5.3	0.500	167.7 ± 1.2	0.459	24.6 ± 0.2	0.418
$p_T(\text{jets}) > 40$ GeV	751.0 ± 5.3	0.999	167.5 ± 1.2	0.999	24.6 ± 0.2	0.999
$p_T^{\ell_1} > 60$ GeV, $p_T^{\ell_2} > 53$ GeV	735.1 ± 5.3	0.979	164.8 ± 1.2	0.984	24.4 ± 0.2	0.992
$\Delta R_{\ell j} > 0.4$	735.1 ± 5.3	1.000	164.8 ± 1.2	1.000	24.4 ± 0.2	1.000
$M_{\ell\ell} > 200$ GeV	717.4 ± 5.2	0.976	162.5 ± 1.2	0.986	24.2 ± 0.2	0.992
$M_{\ell\ell jj} > 600$ GeV	717.0 ± 5.2	0.999	162.5 ± 1.2	1.000	24.2 ± 0.2	1.000
Muon channel	Events	ε	Events	ε	Events	ε
Initial	1507.8	-	366.2	-	58.9	-
$N_{\text{jets}} \geq 2$	1403.2 ± 3.7	0.931	346.7 ± 0.8	0.947	56.1 ± 0.1	0.953
$N_\ell \geq 2$	1213.0 ± 5.4	0.864	300.8 ± 1.3	0.867	46.3 ± 0.2	0.824
$p_T(\text{jets}) > 40$ GeV	1145.3 ± 5.6	0.944	285.7 ± 1.3	0.950	44.5 ± 0.2	0.963
$p_T^{\ell_1} > 60$ GeV, $p_T^{\ell_2} > 53$ GeV	1121.7 ± 5.7	0.979	282.5 ± 1.4	0.989	44.2 ± 0.2	0.992
$\Delta R_{\ell j} > 0.4$	1121.7 ± 5.7	1.000	282.5 ± 1.4	1.000	44.2 ± 0.2	1.000
$M_{\ell\ell} > 200$ GeV	1103.7 ± 5.7	0.984	279.5 ± 1.4	0.989	43.9 ± 0.2	0.994
$M_{\ell\ell jj} > 600$ GeV	1103.7 ± 5.7	1.000	279.5 ± 1.4	1.000	43.9 ± 0.2	1.000

Table 6. Cut-flow table relevant to the CMS-EXO-17-011 analysis, for the electron (upper) and muon (lower) channels. Three scenarios are considered, with $M_{W_R} = 2200$, 2800, and 3600 GeV and $M_{N_R} = M_{W_R}/2$. Cut efficiencies are defined in eq. (A.4).

the muon p_T, while electron isolation imposes that the same variable is smaller than 5 GeV. On the other hand, the two jet candidates must each satisfy $p_T > 40$ GeV and $|\eta| < 2.4$. In addition, objects overlapping within $\Delta R > 0.4$ are removed. Signal region definition further constrains that the two leptons have the same flavour, that the invariant mass of the di-lepton system is above 200 GeV (to avoid contamination from the Drell-Yan background), and that the invariant mass of the reconstructed W_R boson $M_{\ell\ell jj}$ is greater than 600 GeV.

Cut-flow tables for selected benchmark scenarios are given in table 6 for both the electron and the muon channels. We consider three W_R-boson masses of 2200, 2800 and 3600 GeV, with the right-handed neutrino mass being fixed in each case to $M_{W_R}/2$. We present the number of events surviving each cut, normalised to an integrated luminosity of 35.9 fb^{-1} and a production cross section evaluated at LO. Moreover, we define the efficiency ε_i after the ith cut by

$$\varepsilon_i = \frac{N_i}{N_{i-1}}, \tag{A.4}$$

where N_k corresponds to the number of events surviving the kth cut. In table 7, we compare the predictions obtained with MadAnalysis 5 for the benchmarks considered with the official results released by the CMS collaboration for different bins in the reconstructed W_R-boson

M_{W_R} ($[M_{\ell\ell jj}^{\min}, M_{\ell\ell jj}^{\max}]$)	MadAnalysis 5	CMS	δ [%]
Electron Channel			
2200 ([1950, 2810])	464.8 ± 3.8	$474.0 \pm 3.7 \pm 44.7$	1.94
2800 ([2530, 3840])	117.2 ± 0.9	$114.1 \pm 0.9 \pm 10.6$	2.71
3600 ([3250, 5170])	17.7 ± 0.1	$19.2 \pm 0.2 \pm 1.8$	7.82
Muon Channel			
2200 ([1860, 2800])	885.9 ± 5.7	$744.0 \pm 4.7 \pm 47.5$	16.02
2800 ([2430, 3930])	211.2 ± 1.4	$177.0 \pm 1.1 \pm 13.1$	16.19
3600 ([3190, 5500])	30.2 ± 0.2	$29.2 \pm 0.2 \pm 2.6$	3.31

Table 7. Comparison between the number of events surviving all cuts as predicted by MadAnalysis 5, and those reported by the CMS collaboration. We consider three scenarios respectively featuring $M_{W_R} = 2200$, 2800 and 3600 GeV, and $M_{N_R} = M_{W_R}/2$. For each scenario, a different bin in the invariant mass of the $\ell\ell jj$ system is considered.

mass. To better quantify the agreement we compute the quantity δ defined by

$$\delta = 100 \times \left| 1 - \frac{n_{\mathrm{MA5}}}{n_{\mathrm{CMS}}} \right|, \tag{A.5}$$

where n_{MA5} (n_{CMS}) refers to the number of events surviving all cuts and with $M_{\ell\ell jj} \in [M_{\ell\ell jj}^{\min}, M_{\ell\ell jj}^{\max}]$ as obtained with MadAnalysis 5 (reported by the CMS collaboration). We observe that our implementation leads to an agreement of about 2%–20%, and can thus be considered as validated.

A.3 CMS-EXO-20-002

The CMS-EXO-17-011 analysis described in section A.2 has been recently superseded by the CMS-EXO-20-002 search exploring similar signs of new physics, but in 138 fb^{-1} of LHC run 2 data. This recent search for W_R-boson production and decay in an $\ell\ell jj$ system via a heavy neutrino includes two classes of search regions. A first one is dedicated to the resolved regime where (at least) four well-separated final-state objects are identified, while a second one focuses on a boosted situation in which (at least) only two well-separated objects are identified. We only consider the former, as it is sufficient for the present study. Report on the recasting of the boosted-regime analysis is left for future work.

The resolved analysis is similar the CMS-EXO-17-011 search, although it embeds a few differences. Events are selected provided that their final state includes exactly two isolated leptons, and at least two small-radius jets (with $R = 0.4$) with $p_T > 40$ GeV and $|\eta| < 0.4$. Among all jets, those with the highest transverse momenta are assumed to originate from the W_R-boson decay, together with the leading and sub-leading charged leptons that are required to satisfy $p_T > 60$ GeV and 53 GeV respectively, and to be within $|\eta| < 2.4$ (and not to satisfy $1.44 < |\eta| < 1.57$ for electrons). Lepton isolation is enforced through a dedicated variable

$$I_\ell \equiv \sum_{i \in \mathrm{tracks}} p_T^i, \tag{A.6}$$

$\{M_{W_R}, M_{N_R}\} = (3000, 1400)$ GeV	CMS		MADANALYSIS		
	Events	ε	Events	ε	δ [%]
Initial	1175.4	-	1174.4	-	-
$N_\ell \geq 2$ with $p_T^\ell > 60$ (53) GeV	379.5	0.323	363.5 ± 3.0	0.309	4.1
≥ 2 AK4 jets with $p_T > 40$ GeV	363.1	0.957	363.0 ± 3.0	0.999	4.4
$\Delta R > 0.4$ between all pairs of objects	355.4	0.979	363.0 ± 3.0	1.000	2.2
$m_{\ell\ell} > 200$ GeV	335.6	0.944	358.3 ± 3.0	0.987	4.5
$m_{\ell\ell jj} > 800$ GeV	335.6	1.000	357.1 ± 3.0	0.997	0.3
$m_{\ell\ell} > 400$ GeV	324.1	0.966	339.5 ± 2.9	0.951	1.6
$\{M_{W_R}, M_{N_R}\} = (4000, 2000)$ GeV	Events	ε	Events	ε	δ [%]
Initial	115.2	-	115.2	-	-
$N_\ell \geq 2$ with $p_T^\ell > 60$ (53) GeV	37.2	0.322	32.9 ± 0.3	0.285	11.5
≥ 2 AK4 jets with $p_T > 40$ GeV	36.0	0.969	32.7 ± 0.3	0.996	2.8
$\Delta R > 0.4$ between all pairs of objects	35.1	0.974	32.7 ± 0.3	1.000	2.6
$m_{\ell\ell} > 200$ GeV	33.2	0.947	32.5 ± 0.3	0.993	4.8
$m_{\ell\ell jj} > 800$ GeV	33.2	1.000	32.5 ± 0.3	0.999	0.1
$m_{\ell\ell} > 400$ GeV	32.5	0.979	31.4 ± 0.3	0.966	1.3
$\{M_{W_R}, M_{N_R}\} = (5000, 3000)$ GeV	Events	ε	Events	ε	δ [%]
Initial	11.8	-	11.8	-	-
$N_\ell \geq 2$ with $p_T^\ell > 60$ (53) GeV	3.8	0.317	3.1 ± 0.0	0.264	16.9
≥ 2 AK4 jets with $p_T > 40$ GeV	3.7	0.987	3.1 ± 0.0	0.999	1.3
$\Delta R > 0.4$ between all pairs of objects	3.6	0.968	3.1 ± 0.0	1.000	3.4
$m_{\ell\ell} > 200$ GeV	3.4	0.947	3.1 ± 0.0	0.997	5.3
$m_{\ell\ell jj} > 800$ GeV	3.4	1.000	3.1 ± 0.0	1.000	0.0
$m_{\ell\ell} > 400$ GeV	3.4	0.988	3.0 ± 0.0	0.974	1.4

Table 8. Cut-flow tables as predicted with MADANALYSIS 5 and as reported by the CMS collaboration, for the analysis of the $eejj$ final state. Three scenarios are considered, with $\{M_{W_R}, M_{N_R}\} = (3000, 1400), (4000, 2000)$ and $(5000, 3000)$ GeV, for which we provide number of events normalised to 138 fb^{-1} and cut-by-cut efficiencies (ε) as defined in eq. (A.4). We also display the level of agreement between the CMS and MADANALYSIS 5 results, as quantified by the δ variabble introduced in eq. (A.5).

where the sum runs over all tracks separated by $\Delta R < 0.3$ from the lepton direction. Lepton definition then requires that $I_\mu < 0.1 p_T^\mu$, and that $I_e < 5$ GeV. Furthermore, all final-state object candidates are imposed not to overlap, and to satisfy $\Delta R > 0.4$. In addition, a good background rejection is guaranteed by a first selection on the di-lepton invariant mass, $M_{\ell\ell} > 400$ GeV, and by a second selection on the invariant mass of the reconstructed W_R-boson candidate (i.e. the invariant mass of the $\ell\ell jj$ system), $M_{\ell\ell jj} > 800$ GeV.

$\{M_{W_R}, M_{N_R}\} = (3000, 1400)$ GeV	CMS		MADANALYSIS		
	Events	ε	Events	ε	δ [%]
Initial	586.6	-	587.2	-	-
$N_\ell \geq 2$ with $p_T^\ell > 60$ (53) GeV	494.5	0.843	498.6 ± 1.9	0.849	0.7
≥ 2 AK4 jets with $p_T > 40$ GeV	473.2	0.957	450.6 ± 2.2	0.904	5.6
$\Delta R > 0.4$ between all pairs of objects	443.1	0.936	450.6 ± 2.2	1.000	6.8
$m_{\ell\ell} > 200$ GeV	420.8	0.950	447.3 ± 2.2	0.993	4.5
$m_{\ell\ell jj} > 800$ GeV	420.7	1.000	447.2 ± 2.2	1.000	0.0
$m_{\ell\ell} > 400$ GeV	407.3	0.968	431.6 ± 2.2	0.965	0.3
$\{M_{W_R}, M_{N_R}\} = (4000, 2000)$ GeV	Events	ε	Events	ε	δ [%]
Initial	57.6	-	57.6	-	-
$N_\ell \geq 2$ with $p_T^\ell > 60$ (53) GeV	49.8	0.864	45.2 ± 0.2	0.786	9.1
≥ 2 AK4 jets with $p_T > 40$ GeV	48.4	0.971	41.8 ± 0.2	0.925	4.8
$\Delta R > 0.4$ between all pairs of objects	45.4	0.940	41.8 ± 0.2	1.000	6.4
$m_{\ell\ell} > 200$ GeV	43.5	0.957	41.7 ± 0.2	0.997	4.2
$m_{\ell\ell jj} > 800$ GeV	43.5	1.000	41.7 ± 0.2	1.000	0.0
$m_{\ell\ell} > 400$ GeV	42.8	0.985	40.7 ± 0.2	0.977	0.8
$\{M_{W_R}, M_{N_R}\} = (5000, 3000)$ GeV	Events	ε	Events	ε	δ [%]
Initial	5.9	-	5.9	-	-
$N_\ell \geq 2$ with $p_T^\ell > 60$ (53) GeV	5.1	0.858	4.4 ± 0.0	0.749	12.7
≥ 2 AK4 jets with $p_T > 40$ GeV	5.0	0.984	4.1 ± 0.0	0.923	6.2
$\Delta R > 0.4$ between all pairs of objects	4.7	0.940	4.1 ± 0.0	1.000	6.4
$m_{\ell\ell} > 200$ GeV	4.5	0.960	4.1 ± 0.0	0.997	3.9
$m_{\ell\ell jj} > 800$ GeV	4.5	1.000	4.1 ± 0.0	1.000	0.0
$m_{\ell\ell} > 400$ GeV	4.5	0.991	4.0 ± 0.0	0.982	0.9

Table 9. Same as in table 8 but for the $\mu\mu jj$ channel.

A comparison between the results obtained with our implementation of the CMS-EXO-20-002 analysis in MADANALYSIS 5 and the official results as released by the CMS collaboration are shown in tables 8 (for the electron channel) and 9 (for the muon channel). In these tables, we consider three scenarios defined by $\{M_{W_R}, M_{N_R}\} = (3000, 1400)$, $(4000, 2000)$ and $(5000, 3000)$ GeV. To quantify the agreement between our predictions with MADANALYSIS 5 and the official results provided by the CMS collaboration, we make use of the δ variable introduced in eq. (A.5). An amazingly good agreement between the two is found, which validates our implementation.

References

[1] J.C. Pati and A. Salam, *Lepton Number as the Fourth Color*, *Phys. Rev. D* **10** (1974) 275 [INSPIRE].

[2] R.N. Mohapatra and J.C. Pati, *Left-Right Gauge Symmetry and an Isoconjugate Model of CP Violation*, *Phys. Rev. D* **11** (1975) 566 [INSPIRE].

[3] G. Senjanović and R.N. Mohapatra, *Exact Left-Right Symmetry and Spontaneous Violation of Parity*, *Phys. Rev. D* **12** (1975) 1502 [INSPIRE].

[4] G. Senjanović, *Spontaneous Breakdown of Parity in a Class of Gauge Theories*, *Nucl. Phys. B* **153** (1979) 334 [INSPIRE].

[5] R.N. Mohapatra and G. Senjanović, *Neutrino Mass and Spontaneous Parity Nonconservation*, *Phys. Rev. Lett.* **44** (1980) 912 [INSPIRE].

[6] R.N. Mohapatra and G. Senjanović, *Neutrino Masses and Mixings in Gauge Models with Spontaneous Parity Violation*, *Phys. Rev. D* **23** (1981) 165 [INSPIRE].

[7] Y. Cai, T. Han, T. Li and R. Ruiz, *Lepton Number Violation: Seesaw Models and Their Collider Tests*, *Front. in Phys.* **6** (2018) 40 [arXiv:1711.02180] [INSPIRE].

[8] V. Cirigliano, A. Kurylov, M.J. Ramsey-Musolf and P. Vogel, *Lepton flavor violation without supersymmetry*, *Phys. Rev. D* **70** (2004) 075007 [hep-ph/0404233] [INSPIRE].

[9] K. Hsieh, K. Schmitz, J.-H. Yu and C.-P. Yuan, *Global Analysis of General* $\mathrm{SU}(2) \times \mathrm{SU}(2) \times \mathrm{U}(1)$ *Models with Precision Data*, *Phys. Rev. D* **82** (2010) 035011 [arXiv:1003.3482] [INSPIRE].

[10] M. Blanke, A.J. Buras, K. Gemmler and T. Heidsieck, $\Delta F = 2$ *observables and* $B \to X_q \gamma$ *decays in the Left-Right Model: Higgs particles striking back*, *JHEP* **03** (2012) 024 [arXiv:1111.5014] [INSPIRE].

[11] V. Bernard, S. Descotes-Genon and L. Vale Silva, *Constraining the gauge and scalar sectors of the doublet left-right symmetric model*, *JHEP* **09** (2020) 088 [arXiv:2001.00886] [INSPIRE].

[12] G. Beall, M. Bander and A. Soni, *Constraint on the Mass Scale of a Left-Right Symmetric Electroweak Theory from the* $K_L - K_S$ *Mass Difference*, *Phys. Rev. Lett.* **48** (1982) 848 [INSPIRE].

[13] R.N. Mohapatra, G. Senjanović and M.D. Tran, *Strangeness Changing Processes and the Limit on the Right-handed Gauge Boson Mass*, *Phys. Rev. D* **28** (1983) 546 [INSPIRE].

[14] G. Ecker, W. Grimus and H. Neufeld, *Higgs Induced Flavor Changing Neutral Interactions in* $\mathrm{SU}(2)_l \times \mathrm{SU}(2)_r \times \mathrm{U}(1)$, *Phys. Lett. B* **127** (1983) 365 [*Erratum ibid.* **132** (1983) 467] [INSPIRE].

[15] G. Ecker and W. Grimus, *Mass Mixing, CP Violation and Left-right Symmetry for Heavy Neutral Mesons*, *Z. Phys. C* **30** (1986) 293 [INSPIRE].

[16] J.M. Frere et al., $K^0 \bar{K}^0$ *in the* $\mathrm{SU}(2)_L \times \mathrm{SU}(2)_R \times \mathrm{U}(1)$ *model of CP violation*, *Phys. Rev. D* **46** (1991) 337 [INSPIRE].

[17] P. Ball, J.M. Frere and J. Matias, *Anatomy of mixing induced CP asymmetries in left-right symmetric models with spontaneous CP violation*, *Nucl. Phys. B* **572** (2000) 3 [hep-ph/9910211] [INSPIRE].

[18] A. Maiezza, M. Nemevšek, F. Nesti and G. Senjanović, *Left-Right Symmetry at LHC*, *Phys. Rev. D* **82** (2010) 055022 [arXiv:1005.5160] [INSPIRE].

[19] S. Bertolini, A. Maiezza and F. Nesti, *Present and Future K and B Meson Mixing Constraints on TeV Scale Left-Right Symmetry*, *Phys. Rev. D* **89** (2014) 095028 [arXiv:1403.7112] [INSPIRE].

[20] G. Ecker, W. Grimus and H. Neufeld, *The Neutron Electric Dipole Moment in Left-right Symmetric Gauge Models*, *Nucl. Phys. B* **229** (1983) 421 [INSPIRE].

[21] J.M. Frere et al., *The neutron electric dipole moment in left-right symmetric models*, *Phys. Rev. D* **45** (1992) 259 [INSPIRE].

[22] F. Xu, H. An and X. Ji, *Neutron Electric Dipole Moment Constraint on Scale of Minimal Left-Right Symmetric Model*, *JHEP* **03** (2010) 088 [arXiv:0910.2265] [INSPIRE].

[23] V. Cirigliano, W. Dekens, J. de Vries and E. Mereghetti, *An ϵ' improvement from right-handed currents*, *Phys. Lett. B* **767** (2017) 1 [arXiv:1612.03914] [INSPIRE].

[24] M.J. Ramsey-Musolf and J.C. Vasquez, *Left-right symmetry and electric dipole moments. A global analysis*, *Phys. Lett. B* **815** (2021) 136136 [arXiv:2012.02799] [INSPIRE].

[25] V. Cirigliano, S. Gardner and B. Holstein, *Beta Decays and Non-Standard Interactions in the LHC Era*, *Prog. Part. Nucl. Phys.* **71** (2013) 93 [arXiv:1303.6953] [INSPIRE].

[26] M. González-Alonso, O. Naviliat-Cuncic and N. Severijns, *New physics searches in nuclear and neutron β decay*, *Prog. Part. Nucl. Phys.* **104** (2019) 165 [arXiv:1803.08732] [INSPIRE].

[27] W. Dekens et al., *A low-energy perspective on the minimal left-right symmetric model*, *JHEP* **11** (2021) 127 [arXiv:2107.10852] [INSPIRE].

[28] G. Prezeau, M. Ramsey-Musolf and P. Vogel, *Neutrinoless double beta decay and effective field theory*, *Phys. Rev. D* **68** (2003) 034016 [hep-ph/0303205] [INSPIRE].

[29] V. Tello et al., *Left-Right Symmetry: from LHC to Neutrinoless Double Beta Decay*, *Phys. Rev. Lett.* **106** (2011) 151801 [arXiv:1011.3522] [INSPIRE].

[30] M. Nemevšek, F. Nesti, G. Senjanović and V. Tello, *Neutrinoless Double Beta Decay: Low Left-Right Symmetry Scale?*, arXiv:1112.3061 [INSPIRE].

[31] M. Nemevšek, G. Senjanović and V. Tello, *Connecting Dirac and Majorana Neutrino Mass Matrices in the Minimal Left-Right Symmetric Model*, *Phys. Rev. Lett.* **110** (2013) 151802 [arXiv:1211.2837] [INSPIRE].

[32] J. Barry and W. Rodejohann, *Lepton number and flavour violation in TeV-scale left-right symmetric theories with large left-right mixing*, *JHEP* **09** (2013) 153 [arXiv:1303.6324] [INSPIRE].

[33] P.S. Bhupal Dev, S. Goswami and M. Mitra, *TeV Scale Left-Right Symmetry and Large Mixing Effects in Neutrinoless Double Beta Decay*, *Phys. Rev. D* **91** (2015) 113004 [arXiv:1405.1399] [INSPIRE].

[34] G. Bambhaniya, P.S.B. Dev, S. Goswami and M. Mitra, *The Scalar Triplet Contribution to Lepton Flavour Violation and Neutrinoless Double Beta Decay in Left-Right Symmetric Model*, *JHEP* **04** (2016) 046 [arXiv:1512.00440] [INSPIRE].

[35] G. Barenboim, M. Gorbahn, U. Nierste and M. Raidal, *Higgs Sector of the Minimal Left-Right Symmetric Model*, *Phys. Rev. D* **65** (2002) 095003 [`hep-ph/0107121`] [InSPIRE].

[36] A. Maiezza, G. Senjanović and J.C. Vasquez, *Higgs sector of the minimal left-right symmetric theory*, *Phys. Rev. D* **95** (2017) 095004 [`arXiv:1612.09146`] [InSPIRE].

[37] G. Bambhaniya et al., *Left-Right Symmetry and the Charged Higgs Bosons at the LHC*, *JHEP* **05** (2014) 033 [`arXiv:1311.4144`] [InSPIRE].

[38] P.S.B. Dev, R.N. Mohapatra and Y. Zhang, *Probing the Higgs Sector of the Minimal Left-Right Symmetric Model at Future Hadron Colliders*, *JHEP* **05** (2016) 174 [`arXiv:1602.05947`] [InSPIRE].

[39] W. Rodejohann, *Neutrino-less Double Beta Decay and Particle Physics*, *Int. J. Mod. Phys. E* **20** (2011) 1833 [`arXiv:1106.1334`] [InSPIRE].

[40] V. Cirigliano et al., *A neutrinoless double beta decay master formula from effective field theory*, *JHEP* **12** (2018) 097 [`arXiv:1806.02780`] [InSPIRE].

[41] G. Li, M. Ramsey-Musolf and J.C. Vasquez, *Left-Right Symmetry and Leading Contributions to Neutrinoless Double Beta Decay*, *Phys. Rev. Lett.* **126** (2021) 151801 [`arXiv:2009.01257`] [InSPIRE].

[42] J.L. Yang, C.-H. Chang and T.-F. Feng, *Nuclear 0ν2β decays in B − L symmetric SUSY model and in TeV scale left-right symmetric model*, *Commun. Theor. Phys.* **74** (2022) 085202 [`arXiv:2107.01367`] [InSPIRE].

[43] W.-Y. Keung and G. Senjanović, *Majorana Neutrinos and the Production of the Right-handed Charged Gauge Boson*, *Phys. Rev. Lett.* **50** (1983) 1427 [InSPIRE].

[44] M. Nemevšek, F. Nesti, G. Senjanović and Y. Zhang, *First Limits on Left-Right Symmetry Scale from LHC Data*, *Phys. Rev. D* **83** (2011) 115014 [`arXiv:1103.1627`] [InSPIRE].

[45] A. Das, P.S.B. Dev and R.N. Mohapatra, *Same Sign versus Opposite Sign Dileptons as a Probe of Low Scale Seesaw Mechanisms*, *Phys. Rev. D* **97** (2018) 015018 [`arXiv:1709.06553`] [InSPIRE].

[46] M. Nemevšek, F. Nesti and G. Popara, *Keung-Senjanović process at the LHC: From lepton number violation to displaced vertices to invisible decays*, *Phys. Rev. D* **97** (2018) 115018 [`arXiv:1801.05813`] [InSPIRE].

[47] M. Nemevšek and F. Nesti, *Left-right symmetry at an FCC-hh*, *Phys. Rev. D* **108** (2023) 015030 [`arXiv:2306.12104`] [InSPIRE].

[48] ATLAS collaboration, *Search for heavy Majorana or Dirac neutrinos and right-handed W gauge bosons in final states with two charged leptons and two jets at √s = 13 TeV with the ATLAS detector*, *JHEP* **01** (2019) 016 [`arXiv:1809.11105`] [InSPIRE].

[49] ATLAS collaboration, *Search for a right-handed gauge boson decaying into a high-momentum heavy neutrino and a charged lepton in pp collisions with the ATLAS detector at √s = 13 TeV*, *Phys. Lett. B* **798** (2019) 134942 [`arXiv:1904.12679`] [InSPIRE].

[50] CMS collaboration, *Search for a heavy right-handed W boson and a heavy neutrino in events with two same-flavor leptons and two jets at √s = 13 TeV*, *JHEP* **05** (2018) 148 [`arXiv:1803.11116`] [InSPIRE].

[51] CMS collaboration, *Search for heavy Majorana neutrinos in same-sign dilepton channels in proton-proton collisions at √s = 13 TeV*, *JHEP* **01** (2019) 122 [`arXiv:1806.10905`] [InSPIRE].

[52] CMS collaboration, *Search for a right-handed W boson and a heavy neutrino in proton-proton collisions at $\sqrt{s} = 13$ TeV*, *JHEP* **04** (2022) 047 [`arXiv:2112.03949`] [InSPIRE].

[53] M. Frank, Ö. Özdal and P. Poulose, *Relaxing LHC constraints on the W_R mass*, *Phys. Rev. D* **99** (2019) 035001 [`arXiv:1812.05681`] [InSPIRE].

[54] Ö. Özdal, *Loopholes in W_R Searches at the LHC*, in the proceedings of the *11th International Symposium on Quantum Theory and Symmetries*, Montreal, Canada, July 01–05 (2019) [`DOI:10.1007/978-3-030-55777-5_55`] [InSPIRE].

[55] B. Fuks et al., *Majorana neutrinos in same-sign $W^{\pm}W^{\pm}$ scattering at the LHC: Breaking the TeV barrier*, *Phys. Rev. D* **103** (2021) 055005 [`arXiv:2011.02547`] [InSPIRE].

[56] B. Fuks et al., *Probing the Weinberg operator at colliders*, *Phys. Rev. D* **103** (2021) 115014 [`arXiv:2012.09882`] [InSPIRE].

[57] CMS collaboration, *Probing Heavy Majorana Neutrinos and the Weinberg Operator through Vector Boson Fusion Processes in Proton-Proton Collisions at $\sqrt{s} = 13$ TeV*, *Phys. Rev. Lett.* **131** (2023) 011803 [`arXiv:2206.08956`] [InSPIRE].

[58] ATLAS collaboration, *Search for Majorana neutrinos in same-sign WW scattering events from pp collisions at $\sqrt{s} = 13$ TeV*, *Eur. Phys. J. C* **83** (2023) 824 [`arXiv:2305.14931`] [InSPIRE].

[59] M. Mitra, R. Ruiz, D.J. Scott and M. Spannowsky, *Neutrino Jets from High-Mass W_R Gauge Bosons in TeV-Scale Left-Right Symmetric Models*, *Phys. Rev. D* **94** (2016) 095016 [`arXiv:1607.03504`] [InSPIRE].

[60] V. Tello, *Connections between the high and low energy violation of Lepton and Flavor numbers in the minimal left-right symmetric model*, Ph.D. thesis, Scuola Internazionale Superiore di Studi Avanzati (SISSA), I-34136 Trieste, Italy (2012).

[61] J. Chakrabortty, P. Konar and T. Mondal, *Copositive Criteria and Boundedness of the Scalar Potential*, *Phys. Rev. D* **89** (2014) 095008 [`arXiv:1311.5666`] [InSPIRE].

[62] A. Maiezza, M. Nemevšek and F. Nesti, *Perturbativity and mass scales in the minimal left-right symmetric model*, *Phys. Rev. D* **94** (2016) 035008 [`arXiv:1603.00360`] [InSPIRE].

[63] P.S. Bhupal Dev, R.N. Mohapatra, W. Rodejohann and X.-J. Xu, *Vacuum structure of the left-right symmetric model*, *JHEP* **02** (2019) 154 [`arXiv:1811.06869`] [InSPIRE].

[64] G. Chauhan, *Vacuum Stability and Symmetry Breaking in Left-Right Symmetric Model*, *JHEP* **12** (2019) 137 [`arXiv:1907.07153`] [InSPIRE].

[65] Particle Data Group collaboration, *Review of Particle Physics*, *PTEP* **2022** (2022) 083C01 [InSPIRE].

[66] E. Accomando et al., *Interference effects in heavy W'-boson searches at the LHC*, *Phys. Rev. D* **85** (2012) 115017 [`arXiv:1110.0713`] [InSPIRE].

[67] E. Accomando et al., *W' and Z' searches at the LHC*, *PoS* **DIS2013** (2013) 125 [InSPIRE].

[68] ATLAS collaboration, *Search for a heavy charged boson in events with a charged lepton and missing transverse momentum from pp collisions at $\sqrt{s} = 13$ TeV with the ATLAS detector*, *Phys. Rev. D* **100** (2019) 052013 [`arXiv:1906.05609`] [InSPIRE].

[69] CMS collaboration, *Search for new physics in the lepton plus missing transverse momentum final state in proton-proton collisions at $\sqrt{s} = 13$ TeV*, *JHEP* **07** (2022) 067 [`arXiv:2202.06075`] [InSPIRE].

[70] CMS collaboration, *Search for heavy neutrinos and third-generation leptoquarks in hadronic states of two τ leptons and two jets in proton-proton collisions at $\sqrt{s} = 13$ TeV*, *JHEP* **03** (2019) 170 [arXiv:1811.00806] [INSPIRE].

[71] ATLAS collaboration, *Search for new resonances in mass distributions of jet pairs using 139 fb^{-1} of pp collisions at $\sqrt{s} = 13$ TeV with the ATLAS detector*, *JHEP* **03** (2020) 145 [arXiv:1910.08447] [INSPIRE].

[72] ATLAS collaboration, *Search for vector-boson resonances decaying to a top quark and bottom quark in the lepton plus jets final state in pp collisions at $\sqrt{s} = 13$ TeV with the ATLAS detector*, *Phys. Lett. B* **788** (2019) 347 [arXiv:1807.10473].

[73] CMS collaboration, *Search for heavy resonances decaying into a vector boson and a Higgs boson in final states with charged leptons, neutrinos and b quarks at $\sqrt{s} = 13$ TeV*, *JHEP* **11** (2018) 172 [arXiv:1807.02826] [INSPIRE].

[74] ATLAS collaboration, *Search for heavy diboson resonances in semileptonic final states in pp collisions at $\sqrt{s} = 13$ TeV with the ATLAS detector*, *Eur. Phys. J. C* **80** (2020) 1165 [arXiv:2004.14636] [INSPIRE].

[75] Y. Zhang, H. An, X. Ji and R.N. Mohapatra, *Right-handed quark mixings in minimal left-right symmetric model with general CP violation*, *Phys. Rev. D* **76** (2007) 091301 [arXiv:0704.1662] [INSPIRE].

[76] TWIST collaboration, *Precise measurement of parity violation in polarized muon decay*, *Phys. Rev. D* **84** (2011) 032005 [arXiv:1104.3632] [INSPIRE].

[77] J. Alwall et al., *The automated computation of tree-level and next-to-leading order differential cross sections, and their matching to parton shower simulations*, *JHEP* **07** (2014) 079 [arXiv:1405.0301] [INSPIRE].

[78] C. Degrande et al., *UFO — The Universal FeynRules Output*, *Comput. Phys. Commun.* **183** (2012) 1201 [arXiv:1108.2040] [INSPIRE].

[79] L. Darmé et al., *UFO 2.0: the 'Universal Feynman Output' format*, *Eur. Phys. J. C* **83** (2023) 631 [arXiv:2304.09883] [INSPIRE].

[80] A. Alloul et al., *FeynRules 2.0 — A complete toolbox for tree-level phenomenology*, *Comput. Phys. Commun.* **185** (2014) 2250 [arXiv:1310.1921] [INSPIRE].

[81] N.D. Christensen et al., *A comprehensive approach to new physics simulations*, *Eur. Phys. J. C* **71** (2011) 1541 [arXiv:0906.2474] [INSPIRE].

[82] C. Degrande, *Automatic evaluation of UV and R2 terms for beyond the Standard Model Lagrangians: a proof-of-principle*, *Comput. Phys. Commun.* **197** (2015) 239 [arXiv:1406.3030] [INSPIRE].

[83] B. Fuks and R. Ruiz, *A comprehensive framework for studying W′ and Z′ bosons at hadron colliders with automated jet veto resummation*, *JHEP* **05** (2017) 032 [arXiv:1701.05263] [INSPIRE].

[84] P. Artoisenet, R. Frederix, O. Mattelaer and R. Rietkerk, *Automatic spin-entangled decays of heavy resonances in Monte Carlo simulations*, *JHEP* **03** (2013) 015 [arXiv:1212.3460] [INSPIRE].

[85] NNPDF collaboration, *The path to proton structure at 1% accuracy*, *Eur. Phys. J. C* **82** (2022) 428 [arXiv:2109.02653] [INSPIRE].

[86] Z. Sullivan, *Fully Differential W′ Production and Decay at Next-to-Leading Order in QCD*, *Phys. Rev. D* **66** (2002) 075011 [hep-ph/0207290] [INSPIRE].

[87] O. Mattelaer, M. Mitra and R. Ruiz, *Automated Neutrino Jet and Top Jet Predictions at Next-to-Leading-Order with Parton Shower Matching in Effective Left-Right Symmetric Models*, arXiv:1610.08985 [INSPIRE].

[88] M. Cacciari, G.P. Salam and G. Soyez, *The anti-k_t jet clustering algorithm*, *JHEP* **04** (2008) 063 [arXiv:0802.1189] [INSPIRE].

[89] M. Cacciari, G.P. Salam and G. Soyez, *FastJet User Manual*, *Eur. Phys. J. C* **72** (2012) 1896 [arXiv:1111.6097] [INSPIRE].

[90] E. Conte, B. Fuks and G. Serret, *MadAnalysis 5, A User-Friendly Framework for Collider Phenomenology*, *Comput. Phys. Commun.* **184** (2013) 222 [arXiv:1206.1599] [INSPIRE].

[91] E. Conte, B. Dumont, B. Fuks and C. Wymant, *Designing and recasting LHC analyses with MadAnalysis 5*, *Eur. Phys. J. C* **74** (2014) 3103 [arXiv:1405.3982] [INSPIRE].

[92] E. Conte and B. Fuks, *Confronting new physics theories to LHC data with MADANALYSIS 5*, *Int. J. Mod. Phys. A* **33** (2018) 1830027 [arXiv:1808.00480] [INSPIRE].

[93] J.Y. Araz, B. Fuks and G. Polykratis, *Simplified fast detector simulation in MADANALYSIS 5*, *Eur. Phys. J. C* **81** (2021) 329 [arXiv:2006.09387] [INSPIRE].

[94] J.Y. Araz, B. Fuks, M.D. Goodsell and M. Utsch, *Recasting LHC searches for long-lived particles with MadAnalysis 5*, *Eur. Phys. J. C* **82** (2022) 597 [arXiv:2112.05163] [INSPIRE].

[95] CMS collaboration, *Search for a right-handed W boson and a heavy neutrino in proton-proton collisions at $\sqrt{s} = 13$ TeV*, HEPData Collection (2022) [DOI:10.17182/hepdata.114866].

[96] B. Dumont et al., *Toward a public analysis database for LHC new physics searches using MADANALYSIS 5*, *Eur. Phys. J. C* **75** (2015) 56 [arXiv:1407.3278] [INSPIRE].

[97] A. Jueid and B. Fuks, *Implementation of a search for right-handed W-boson and heavy neutrino in the dilepton+dijet channel (138 fb^{-1}; 13 TeV; CMS-EXO-20-002)*, Open Data (2023) [DOI:10.14428/DVN/UMGIDL].

[98] C. Bierlich et al., *A comprehensive guide to the physics and usage of PYTHIA 8.3*, *SciPost Phys. Codeb.* **2022** (2022) 8 [arXiv:2203.11601] [INSPIRE].

[99] A.L. Read, *Presentation of search results: The CL_s technique*, *J. Phys. G* **28** (2002) 2693 [INSPIRE].

[100] J.Y. Araz, M. Frank and B. Fuks, *Reinterpreting the results of the LHC with MadAnalysis 5: uncertainties and higher-luminosity estimates*, *Eur. Phys. J. C* **80** (2020) 531 [arXiv:1910.11418] [INSPIRE].

[101] J. Campbell, R.K. Ellis and R. Röntsch, *Single Top Production in Association with a Z Boson at the LHC*, *Phys. Rev. D* **87** (2013) 114006 [arXiv:1302.3856] [INSPIRE].

[102] F. Demartin et al., *tWH associated production at the LHC*, *Eur. Phys. J. C* **77** (2017) 34 [arXiv:1607.05862] [INSPIRE].

[103] Y.L. Dokshitzer, G.D. Leder, S. Moretti and B.R. Webber, *Better jet clustering algorithms*, *JHEP* **08** (1997) 001 [hep-ph/9707323] [INSPIRE].

[104] M. Wobisch and T. Wengler, *Hadronization corrections to jet cross-sections in deep inelastic scattering*, in the proceedings of the *Workshop on Monte Carlo Generators for HERA Physics (Plenary Starting Meeting)*, Hamburg, Germany, April 27–30 (1998), p. 270–279 [hep-ph/9907280] [INSPIRE].

[105] T. Plehn, M. Spannowsky, M. Takeuchi and D. Zerwas, *Stop Reconstruction with Tagged Tops*, *JHEP* **10** (2010) 078 [arXiv:1006.2833] [INSPIRE].

[106] G. Kasieczka et al., *Resonance Searches with an Updated Top Tagger*, *JHEP* **06** (2015) 203 [arXiv:1503.05921] [INSPIRE].

[107] J.Y. Araz, A. Buckley and B. Fuks, *Searches for new physics with boosted top quarks in the MadAnalysis 5 and Rivet frameworks*, *Eur. Phys. J. C* **83** (2023) 664 [arXiv:2303.03427] [INSPIRE].

[108] L. Heinrich, M. Feickert, G. Stark and K. Cranmer, *pyhf: pure-Python implementation of HistFactory statistical models*, *J. Open Source Softw.* **6** (2021) 2823 [INSPIRE].

[109] G. Cowan, K. Cranmer, E. Gross and O. Vitells, *Asymptotic formulae for likelihood-based tests of new physics*, *Eur. Phys. J. C* **71** (2011) 1554 [*Erratum ibid.* **73** (2013) 2501] [arXiv:1007.1727] [INSPIRE].

[110] A. Jueid and B. Fuks, *Implementation of a search for right-handed W-boson and heavy neutrino in the dilepton+dijet channel (*35.9 fb^{-1}*; 13 TeV; CMS-EXO-17-011)*, Open Data (2023) [DOI:10.14428/DVN/SGOK0J].

[111] CMS collaboration, *Particle-flow reconstruction and global event description with the CMS detector*, 2017 *JINST* **12** P10003 [arXiv:1706.04965] [INSPIRE].

[112] M. Cacciari and G.P. Salam, *Pileup subtraction using jet areas*, *Phys. Lett. B* **659** (2008) 119 [arXiv:0707.1378] [INSPIRE].

[113] CMS collaboration, *Energy Calibration and Resolution of the CMS Electromagnetic Calorimeter in pp Collisions at $\sqrt{s} = 7$ TeV*, 2013 *JINST* **8** P09009 [arXiv:1306.2016] [INSPIRE].

[114] CMS collaboration, *Description and performance of track and primary-vertex reconstruction with the CMS tracker*, 2014 *JINST* **9** P10009 [arXiv:1405.6569] [INSPIRE].

[115] CMS collaboration, *Performance of Electron Reconstruction and Selection with the CMS Detector in Proton-Proton Collisions at $\sqrt{s} = 8$ TeV*, 2015 *JINST* **10** P06005 [arXiv:1502.02701] [INSPIRE].

[116] CMS collaboration, *Performance of the CMS muon detector and muon reconstruction with proton-proton collisions at $\sqrt{s} = 13$ TeV*, 2018 *JINST* **13** P06015 [arXiv:1804.04528] [INSPIRE].